INFLUENCE OF INTERFACE STRUCTURE ON THE NANOTRIBOLOGICAL PROPERTIES OF EXFOLIATED GRAPHENE

A THESIS SUBMITTED TO
THE GRADUATE SCHOOL OF ENGINEERING AND SCIENCE
OF BILKENT UNIVERSITY
IN PARTIAL FULFILLMENT OF THE REQUIREMENTS FOR
THE DEGREE OF
MASTER OF SCIENCE
IN
MECHANICAL ENGINEERING

By
Arda Balkancı
July 2016

INFLUENCE OF INTERFACE STRUCTURE ON THE NANOTRIBOLOGICAL PROPERTIES OF EXFOLIATED GRAPHENE
By Arda Balkancı
July 2016

We certify that we have read this thesis and that in our opinion it is fully adequate, in scope and in quality, as a thesis for the degree of Master of Science.

Mehmet Zeyyad Baykara(Advisor)

Onur Özcan

Cem Çelebi

Approved for the Graduate School of Engineering and Science:

Levent Onural
Director of the Graduate School

ABSTRACT

INFLUENCE OF INTERFACE STRUCTURE ON THE NANOTRIBOLOGICAL PROPERTIES OF EXFOLIATED GRAPHENE

Arda Balkancı
M.S. in Mechanical Engineering
Advisor: Mehmet Zeyyad Baykara
July 2016

On the nano- and micro-scale, conventional liquid-based lubrication cannot be utilized to minimize friction due to excessive surface tension and related effects. To overcome this limitation, solid lubricants suitable for use in nano- and micro-scale systems are needed. Being a two-dimensional material with outstanding mechanical properties, graphene emerges as a promising candidate for this purpose.

Motivated as above, this M.S. thesis presents a comprehensive investigation of the nanotribological properties of mechanically-exfoliated graphene conducted via atomic force microscopy (AFM), whereby special emphasis is placed on the effect of interface structure.

Graphene samples ranging from single- to few-layers were fabricated using the mechanical exfoliation method and transferred onto Si/SiO_2 substrates. By utilizing optical microscopy and Raman spectroscopy, graphene flakes exhibiting single- and bi-layer regions were located and identified. Furthermore, using topographical maps and associated profiles obtained via AFM, 3-, 4-layer and bulk graphite regions were found. Moreover, AFM probes were calibrated both for accurate normal force readings, and for obtaining quantitative friction force data from lateral force measurements conducted via contact-mode AFM under ambient conditions.

Following sample preparation, identification and probe calibration, experiments aimed at measuring the effect of applied load on friction of single- and 2-, 3-, 4-layers of graphene were performed, confirming previous results reported

in the literature as explained by the *puckering* phenomenon. Additionally, the effect of tip radius and thus, contact area, on the frictional behavior of graphene was quantitatively measured. In particular, thermal evaporation- and PECS (precision etching coating system)-based coating of gold onto AFM probes were utilized to modify tip radii. Results led to the determination of a new parameter affecting friction on graphene: interface roughness. In collaboration with scientists from UC Merced who performed molecular dynamics simulations complementing the experiments presented here, the effect of substrate roughness, which may be in addition to, or dominant over, the puckering phenomenon, was analyzed in terms of the frictional behavior of graphene. Presented experimental results provide a new perspective towards the layer-dependent frictional behavior of graphene, underlining the influence of substrate roughness in addition to the phenomenon of puckering that is well-studied in the literature.

Keywords: Graphene, Nanotribology, Atomic force microscopy, Friction force microscopy, Lateral fore microscopy, Solid lubricant, Puckering, Substrate roughness.

ÖZET

ARAYÜZ YAPISININ MEKANİK SOYMA YÖNTEMİYLE ELDE EDİLEN GRAFENİN NANOTRİBOLOJİK ÖZELLİKLERİNE ETKİSİ

Arda Balkancı
Makine Mühendisliği, Yüksek Lisans
Tez Danışmanı: Mehmet Zeyyad Baykara
Temmuz 2016

Nano ve mikro ölçekte sürtünmeyi en aza indirgemek amacıyla sıvı kayganlaştırıcıların kullanımı, yüksek seviyelerde gerçekleşen yüzey gerilimi ve ilgili etkilerden dolayı mümkün olmamaktadır. Bu kısıtlamayı aşmak için nano ve mikro boyutlu sistemlerde kullanıma uygun katı kayganlaştırıcılara ihtiyaç duyulmaktadır. Üstün mekanik özelliklere sahip iki boyutlu bir malzeme olan grafen, bu amaç için uygun bir aday olarak ortaya çıkmaktadır.

Yukarıda sunulan argümanlar ışığında, bu yüksek lisans tezi, mekanik soyma yöntemiyle elde edilen grafenin nanotribolojik özelliklerinin atomik kuvvet mikroskopisi (AKM) vasıtasıyla incelendiği ve özellikle arayüz yapısının etkisine vurgu yapılan kapsamlı bir araştırma sunmaktadır.

Mekanik soyma yöntemi ile tek- ve az-katman grafen numuneler oluşturulup Si/SiO_2 alttaşlar üzerine aktarılmıştır. Optik mikroskopi ve Raman spektroskopisi kullanılarak, tek- ve çift-katman grafen numuneler teşhis edilmiş ve yerleri saptanmıştır. Ayrıca, AKM yöntemiyle elde edilen topografik haritalar ve ilintili kesitler kullanılarak 3- ve 4-katman grafen numuneler ile yığın grafit olarak tanımlanabilecek bölgeler bulunmuştur. Dahası, AKM uçları oda koşullarında temaslı kipte kullanılacak şekilde, hem hassas normal kuvvet ölçümleri almak, hem de yanal kuvvet ölçümlerinden kantitatif sürtünme kuvveti verileri elde edebilmek adına kalibre edilmiştir.

Numune hazırlama, tanımlama ve AKM uç kalibrasyonunun ardından, uygulanan dikey kuvvetin tek-, 2-, 3-, ve 4-katman grafenin sergilediği sürtünme davranışına etkisini belirlemek adına deneyler gerçekleştirilmiş, elde edilen

sonuçlar literatürde rapor edilen ve *buruşma* etkisiyle açıklanan mevcut verileri doğrulamıştır. Ek olarak, AKM uç yarıçapının ve dolayısıyla temas alanının grafenin sürtünme davranışına olan etkisi kantitatif olarak değerlendirilmiştir. Bu amaçla, ısıl buharlaştırma ve PECS (hassas dağlama ve kaplama sistemi) yöntemleri kullanılarak AKM uçları üzerine altın kaplanmış ve uç yarıçapları böylece büyütülmüştür. Bu şekilde elde edilen deney sonuçları, grafenin sürtünme özelliklerini etkileyen yeni bir değişkenin tespitini sağlamıştır: arayüz pürüzlülüğü. UC Merced bünyesinde çalışmalarını yürüten bilim insanlarıyla iş birliği sonucu elde edilen ve burada sunulan deneysel sonuçları destekleyen moleküler dinamik simülasyonları da kullanarak, alttaş pürüzlülüğünün grafenin sürtünme davranışına etkisi analiz edilmiştir. Elde edilen sonuçlar, bahsi geçen etkinin, buruşma etkisine ek olarak veya ona baskın olacak şekilde tezahür ettiğini ortaya koymaktadır. Sunulan deneysel sonuçlar, grafenin katman sayısına bağlı sürtünme davranışında, literatürde iyi incelenmiş olan buruşma etkisine ek olarak alttaş pürüzlülüğünün de etkisini vurgulayan yeni bir bakış açısı getirmektedir.

Anahtar sözcükler: Grafen, Nanotriboloji, Atomik kuvvet mikroskopisi, Sürtünme kuvvet mikroskopisi, Yanal kuvvet mikroskopisi, Katı kayganlaştırıcı, Buruşma, Alttaş pürüzlülüğü.

Acknowledgement

Before anything else, I would like to express how grateful I am to have Prof. Mehmet Zeyyad Baykara as my academic advisor, who has supported and advised me throughout my dissertation immensely, with his never-ending enthusiasm for research. Working with him was a privileged experience, as he has provided me everything I needed and much more for my research, along with great involvements such as a communicating research group environment, international conferences and collaboration with researchers from other universities. His inspiring success at young age has also motivated me greatly to keep pursuing an academic path. Once again I thank him for his presence and guidance.

Within our Scanning Probe Microscopy (SPM) research group, I have made many friends who were ambitious researchers as well. I would like to thank all our group members, Tuna Demirbaş, Ebru Cihan, Tarek Abdelwahab, Alper Özoğul, Berkin Uluutku, Zeynep Melis Süar and Verda Saygın for always being there for a different point of view to solve a problem and friendly chats in the lab.

I also wish to mention how lucky I am to have such great friends, especially friends that I have made during my education in Bilkent, and the ones that I have met online, with whom I have spent countless hours. Thank you all for the stress relieving fun times we had.

Furthermore, I wish to thank my family for giving me a fantastic life to live for and letting me be whoever I wanted to be. I owe an unimaginable amount to my parents and my sister, who have done everything they can for me my whole life. I also thank our lovely family cat for distracting me whenever she could.

Last but not least, I wish to express my gratefulness and unending love for my special other Ayşe Melis Aygar, for always being by my side and sharing both the exhausting and the enjoyable times throughout my research. I wish her the best of luck in her dissertation as well, for I am excited in a future of doctoral studies and much more together with her.

To my current and future family

Contents

List of Figures

List of Tables

Chapter 1

Introduction

1.1 Tribology: Friction, Lubrication and Wear

Friction is a universal fact of nature which both helps and hinders the various aspects of life. Without friction, we would not be able to walk, grab objects or play stringed instruments. Moreover, if it were not for friction, our world would be readily demolished by asteroid impacts. On the other hand, friction plays an unfavorable role in a multitude of mechanical processes due to the dissipation of energy that it unavoidably leads to, as well as associated consequences such as wear. For instance, friction severely limits the efficiency of combustion engines used in over 1 billion vehicles worldwide on a daily basis, causing drastic economic and environmental impact. As such, even minute improvements in frictional behavior of such systems would yield favorable outcomes in terms of, e.g., fuel consumption and consequently, carbon emissions [1-4].

It is commonly accepted that documented involvement of mankind with friction dates back to the time of the ancient Egyptians (∼1800 B.C.), who used natural lubricants to aid the transportation of large statues from one location to another, as described on a now-famous drawing found on the archaeological site of El-Bersheh [1-3]. Even before the time of the Egyptians, some of the earliest and

most important discoveries of mankind –including the ability to controllably start fires and the invention of the wheel– were aided or motivated by the phenomenon of friction.

While friction has largely remained a topic of empirical (i.e., practical) involvement in ancient times, the approach toward the subject started to change fundamentally thanks to work done by none other than Leonardo da Vinci (1452-1519), who performed the first systematic experiments about friction by using blocks sliding on inclined planes. Despite the fact that da Vinci was indeed able to introduce the concept of the *coefficient of friction* and determine that friction does not depend on the *apparent* contact area, he did not publish his work. His studies as detailed in his notes only resurfaced in 1979, thanks to work by Duncan Dowson [5]. More than a century after da Vinci's experimental work, Robert Hooke (1635-1703) investigated rolling friction and adhesion. Contemporarily with Hooke, Guillaume Amontons (1663-1705) –without knowing about da Vinci's discoveries on friction– re-introduced the conventional friction laws that we still learn today in high school, namely that **(i)** the friction force is directly proportional to normal load, and **(ii)** the friction force is independent of the apparent contact area [6]. These two observations together may be formulated as:

$$F_f = \mu F_n \tag{1.1}$$

where F_f is the friction force, μ is the coefficient of friction (i.e., the proportionality constant) that is taken to depend only on material and structural properties of the sliding surfaces, and F_n is the normal load.

In the period that followed Amontons' discoveries, the difference of static and kinetic friction was observed by Leonhard Euler (1707-1783); and Charles-Augustin de Coulomb (1736-1806) was able to build on the understanding of kinetic friction by showing that it is independent of sliding velocity (which later turned out to be, strictly speaking, not true) [1, 2].

As the reader can see from the paragraphs above, over the course of history, the subject of friction has evolved from its practical roots to an actual field of scientific enquiry. Of course, it is not possible to think of friction without one of its most obvious consequences: wear. Additionally, as discussed earlier, the reduction of friction and wear in mechanical systems is of drastic importance and this goal is typically achieved by lubrication. Therefore, it makes sense to think of friction, wear and lubrication in a combined fashion. Following this line of thought, Peter Jost has introduced the scientific term *tribology* (based on the Greek word *tribos*, which means "to rub") in 1966 [2], which means *the study of friction, lubrication and wear.*

1.2 Nanotribology

In the 20^{th} century, Frank Philip Bowden (1903-1968) and David Tabor (1913-2005) –who are considered to be two of the founding fathers of modern tribology– observed that the *real* contact area between two surfaces "touching" each other is actually much (orders of magnitude) smaller than the apparent contact area. This observation is based on the fact that all surfaces exhibit topographical roughness on small length scales (down to the nanometer scale) no matter how smooth they may appear to the naked eye, and therefore may be thought of as a collection of individual *asperities* [7] (see Figure 1.1). As such, the real contact area is simply the sum of the contact areas formed by individual asperities of the two surfaces that are touching each other. The puzzling observation that friction is found to depend linearly on normal load, but not the (*apparent*) contact area, can also be explained by this picture: As the normal load acting between two surfaces in contact increases, so does the *real* contact area due to **(i)** an increase in asperity deformations and **(ii)** the fact that the number of asperity contacts increases [8]. So, in fact, an increase in normal load causes a proportional increase in *real* contact area, which in turn increases friction proportionally (simply due to the fact that there is more physical interaction between the surfaces now). On the other hand, if the normal load is kept constant, but the apparent contact area is, for instance, doubled; friction remains the same as the number of asperity

contacts has now increased, but the pressure (and hence, the deformation and contact area) associated with each asperity pair has now reduced (leading to a smaller degree of physical interaction at each asperity contact). Hence, the observed independence of friction from apparent contact area.

As the detailed topographical characterization of all surfaces sliding against each other with high resolution is not possible for every physical scenario, the multi-asperity character of surfaces and the associated distinction between apparent and real contact area brings considerable difficulties to the prediction and control of friction for realistic applications. To gain fundamental insight into friction, it is therefore desirable to isolate and focus on a *single asperity*, preferably with nanometer-scale dimensions. As explained below, this idea can now be realized thanks to the invention of the atomic force microscope (AFM) in 1986 [9], and it is now possible to perform friction experiments at nanometer-scale single-asperity contact geometries, rather than macroscopic multi-asperity geometries that form between conventional material surfaces [10, 11]. Thus, the field of *nanotribology* is born.

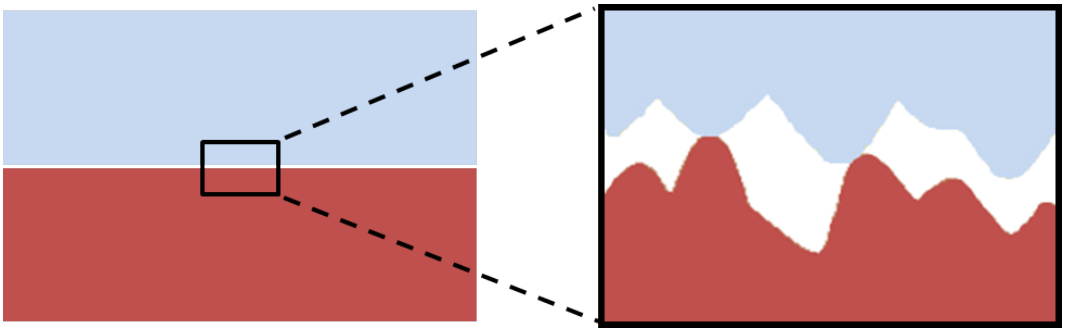

Figure 1.1: Illustration of apparent contact area (left) and actual contact area (right) forming at the multi-asperity interface.

1.2.1 Atomic Force Microscopy

As explained in the previous section, AFM is the main experimental tool that enabled the establishment of the field of nanotribology. Invented by Gerd Binnig and co-workers in 1986 [9], AFM is a member of the scanning probe microscopy

(SPM) family of techniques (which, e.g., also includes scanning tunneling microscopy [12]) that specifically relies on the detection of atomic-scale interaction forces between a sample surface and a sharp tip (or in other words, the *probe*) for imaging and spectroscopy. Most importantly, AFM allows the measurement of the surface topography of various samples on the sub-nm scale, by laterally scanning the very sharp probe over the sample surface, much like a traditional record player. The sharp probe itself is attached to a micro-machined cantilever which acts as a soft spring (with spring constants typically smaller than 1 N/m) that deflects in response to tip-sample interaction forces. By detecting the tiny deflections of the cantilever optically, forces experienced by the probe may be precisely determined (with sub-nN sensitivity); and by employing feedback loops targeted at keeping the tip-sample interaction force constant during scanning, sub-nm scale topographical maps of surfaces may be obtained [13].

AFM cantilevers are usually fabricated out of silicon (Si) or silicon nitride (Si_3N_4) using common micro-fabrication (e.g., photolithography and etching) techniques, where the probe tip apexes can be manufactured to be so sharp that the related radius of curvature is only a few nm. A scanning electron microscopy (SEM) image of a commercial AFM cantilever (together with the sharp probe) is shown in Figure 1.2.

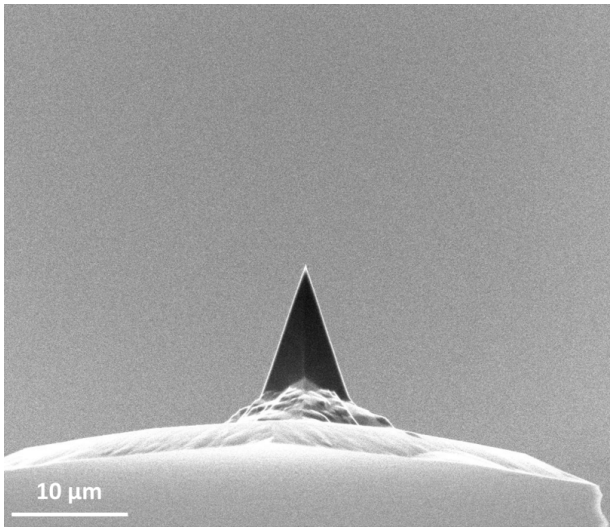

Figure 1.2: Scanning electron microscopy image of a conventional AFM cantilever.

There are multiple operating modes of AFM, including contact, non-contact and tapping modes. Employing the various modes, the AFM can, e.g., **(i)** map the topography of a surface with sub-nm resolution, **(ii)** measure adhesion and stiffness by performing force spectroscopy, and **(iii)** measure magnetic, electrostatic, or friction forces (and more) in a targeted fashion. All the experimental work presented in this thesis has been performed using conventional contact-mode operation, which allows the simultaneous measurement of sample topography and friction forces experienced by the AFM probe.

The basic working principle of an AFM operating in contact mode is as follows: The cantilever with the sharp probe tip is approached to the sample surface using a piezoelectric scanner in a controlled fashion until contact is established. Subsequently, the probe is scanned laterally on the sample surface, by employing the piezoelectric scanner again. The lateral extent of scanned regions on the sample surface typically ranges from a few nm to tens of μm. During the scanning process, the cantilever deflects in the z direction due to the repulsive, normal (i.e., vertical) force interactions between the atoms of the probe and the sample surface. This deflection is detected by a laser beam reflecting from the topside of the cantilever, which then shines onto a position-sensitive photo-detector (PSPD) featuring four equal-sized regions or *quadrants* (see Figure 1.3). The laser spot on the PSPD is initially adjusted to be at the center, so that any deflection of the cantilever in the z direction causes the laser spot to move up or down on the PSPD, which is directly recorded as a voltage difference between the top and bottom regions of the PSPD. When calibrated, this voltage difference is translated into deflection values and consequently, normal interaction forces (F_n) between tip and sample. The determination of F_n which causes the cantilever to deflect in the z direction is performed via the following equation:

$$F_n = \theta_z \left((A + B) - (C + D) \right) \tag{1.2}$$

where θ_z is the force calibration coefficient in the z direction (which is the product of the cantilever spring constant and the photo-detector sensitivity in nm/V); and A, B, C, D are the individual voltages recorded on the quadrants of

the PSPD (A and B being the top, C and D being the bottom quadrants).

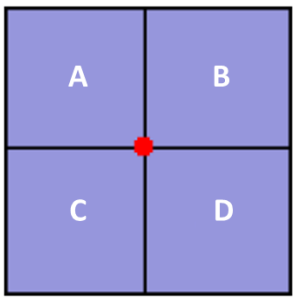

Figure 1.3: A sketch of the 4-quadrant PSPD and the laser spot at the center [14].

During contact-mode scanning, the normal tip-sample interaction force is kept constant using a feedback loop that adjusts the position of the sample in the z direction. By recording the changes in vertical sample position while scanning the surface, high-resolution topographical maps are obtained (see Figure 1.4 for a simple schematic of the AFM setup).

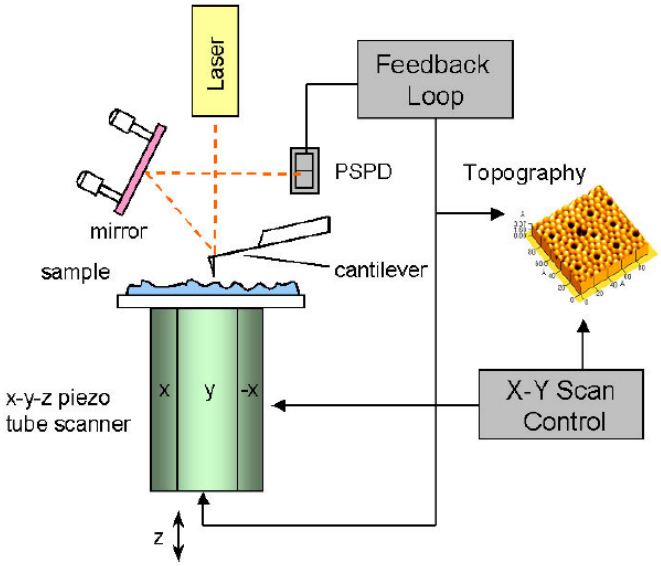

Figure 1.4: A simple schematic illustrating the main operational principle of AFM [14].

1.2.2 Lateral Force Measurement and Friction Force Microscopy

While operating in contact mode, the AFM is not only able to record *deflections* of the cantilever in the vertical z direction used to trace surface topography, but also its torsional *twisting*, which is caused by lateral forces acting at the probe apex due to friction between the tip and the sample. This twisting causes the laser beam reflecting off the topside of the cantilever to move laterally along the left-right axis of the PSPD. Similarly to the measurement of normal forces, by recording the voltage differences between the left and right regions of the PSPD, lateral forces acting on the probe tip can be determined. By standardized calibration techniques explained in Chapter 3, voltage differences between the left and right regions of the PSPD arising due to lateral forces can be converted into actual force values. This operation is performed by the following calculation:

$$F_l = \alpha \left((A + C) - (B + D) \right) \tag{1.3}$$

where α is the lateral force calibration constant, obtained by the calibration methods explained in Chapter 3.

As mentioned in the previous section, before each measurement, the laser beam reflecting off the backside of the cantilever is purposely placed on the exact center of the PSPD to set the starting values for normal and lateral forces as zero. However, during measurements, the initial reference position may change due to cross-talk with normal-force-induced deflections, hampering the accurate detection of lateral force data. To work around this issue, friction forces (F_f) are always calculated by determining the *half-width* (W) of *friction loops* formed by the recording of lateral forces in the forward and backward scan directions ($F_{l,forward}$ and $F_{l,backward}$, respectively), as shown in Figure 1.5 [15]:

$$F_f = \frac{F_{l,forward} - F_{l,backward}}{2} \tag{1.4}$$

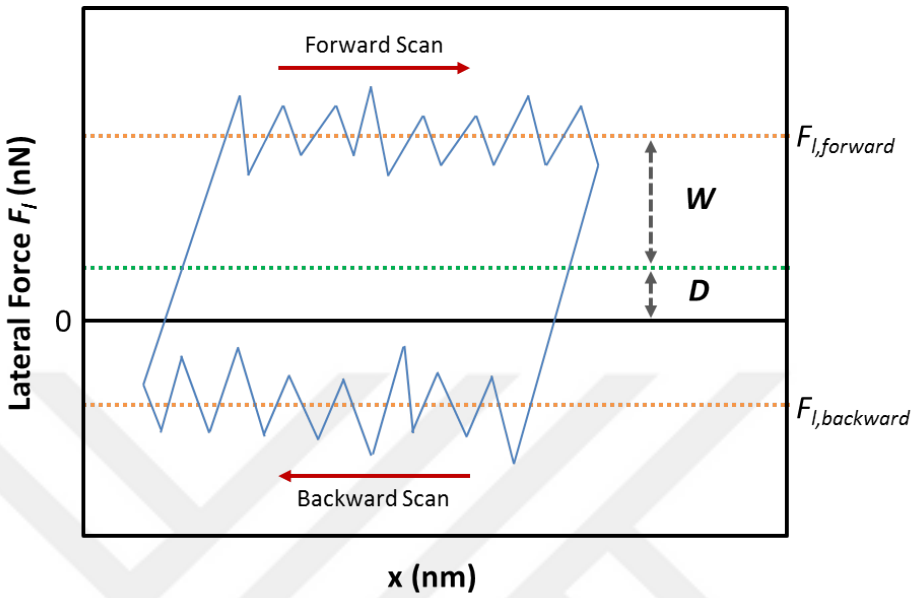

Figure 1.5: An illustration of a friction loop, showing the lateral force signals of the forward and backward scans, the half width of the loop, and the offset value.

The offsets (D) in reference laser spot position can also be calculated, by determining how much the center of the friction loop has swayed from its initial position of zero (again, please refer to Figure 1.5), as by the following equation:

$$D = \frac{F_{l,forward} + F_{l,backward}}{2} \tag{1.5}$$

An important point to note is the fact that the forward and backward lateral force signals have opposite signs. The underlying reason is the opposite sense in which cantilever twisting (clockwise vs. counter-clockwise) occurs while scanning the sample surface in opposite directions, which consequently leads to a lateral displacement of the laser spot on the PSPD in opposing directions for the two scan types.

Finally, to conclude this section, the reader is kindly referred to Figure 1.6 for an illustrative demonstration of topography and lateral force signals that would be recorded on a model surface during contact-mode scanning.

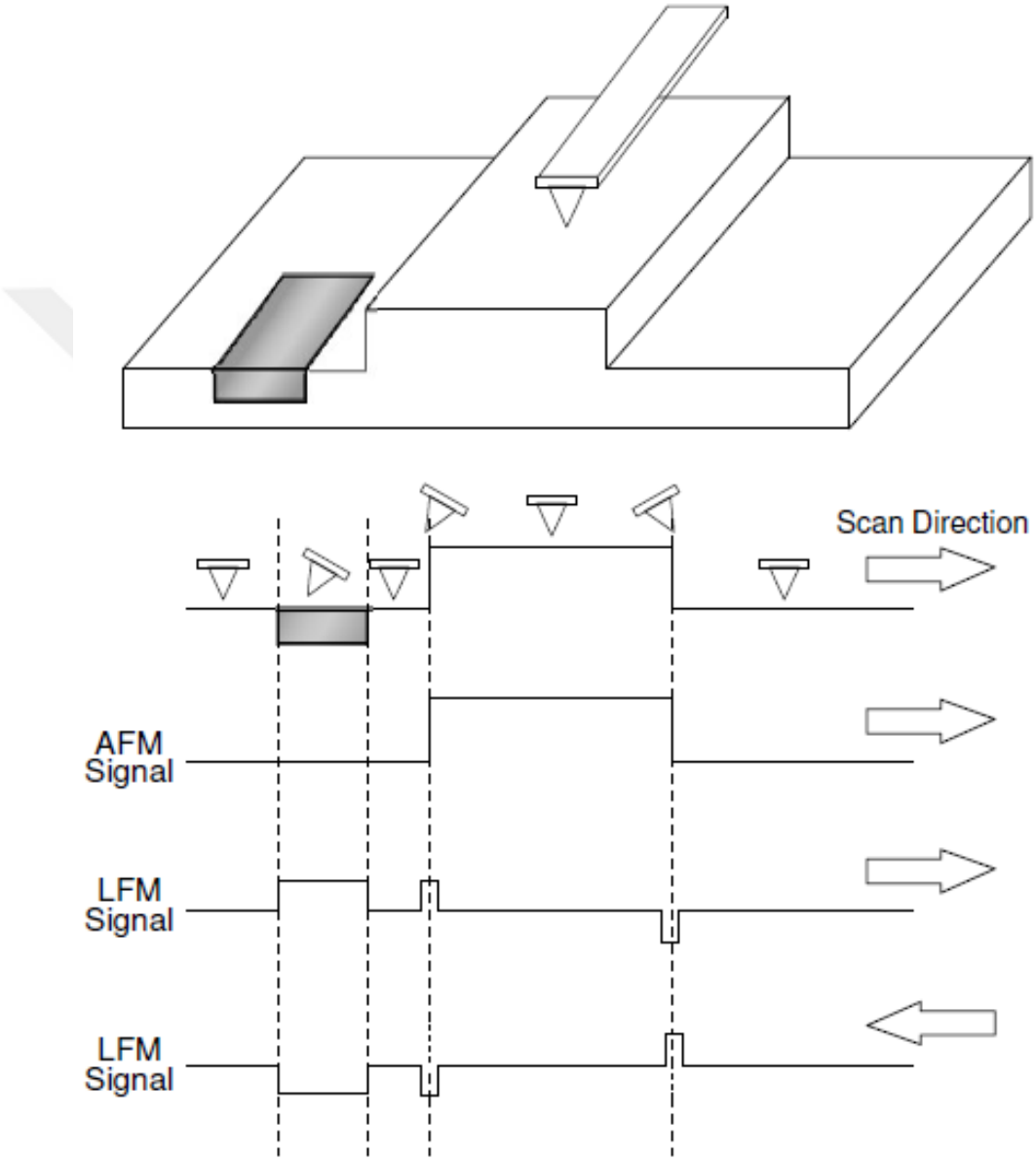

Figure 1.6: A schematic illustration of a model sample surface and corresponding topography (AFM) and lateral force (LFM) signals recorded during contact-mode scanning. For the darker region with high friction coefficient, the topography signal does not change; however the LFM signal shows a plateau (opposite sense for the two scanning directions) due to the additional twisting of the cantilever. For the flat terrace in the middle, the topography signal traces the surface as it is, whereas the LFM signals only peak or valley at the points where the cantilever instantaneously impacts with or drops off the step edges [14].

1.3 Graphene

Discovered in 2004 by Konstantin Novoselov and Andre Geim, graphene is a peculiar *two-dimensional* (2D) material [16]. It is an allotrope of carbon in the form of a single-atom-thick sheet composed of carbon atoms arranged in a honeycomb lattice. Alternatively, graphene may be thought of as a single isolated layer of bulk graphite (Figure 1.7). In the first published work where graphene was deliberately studied [16], the so-called *Scotch-Tape method* (or, i.e., mechanical exfoliation) was employed to produce samples (as explained in Chapter 2 of this thesis). Since the method is easily applicable virtually in any laboratory environment, many research groups around the world have focused their efforts in the last decade on the characterization of the remarkable physical properties of graphene and the realization of related applications. In fact, a whole new class of 2D materials was discovered soon after graphene (silicene, phosphorene, etc.) which changed the landscape of research in multiple disciplines of physics, chemistry and engineering. Based on the intense scientific interest and insight that it generated in a relatively short amount of time [17, 18], the discovery of graphene led to the awarding of the 2010 Nobel Prize in Physics to Novoselov and Geim.

1.3.1 Physical Properties

Graphene is often referred to as the "wonder material" due to its exceptional physical properties. As mentioned above, it is essentially a 2D sheet of carbon atoms with a honeycomb lattice structure, where the individual atoms are bonded with each other via strong covalent bonds featuring sp^2 hybridization. In bulk graphite, individual graphene layers are held together by weak van der Waals interactions, resulting in a spacing of $\sim$3.4 Å between the layers.

In terms of its electrical properties, graphene is quite unique: It is a zero-bandgap semiconductor with a very high electron mobility of $\sim$10,000 $cm^2/V{\cdot}s$ under ambient conditions [20], whereby electrons behave as *massless* Dirac

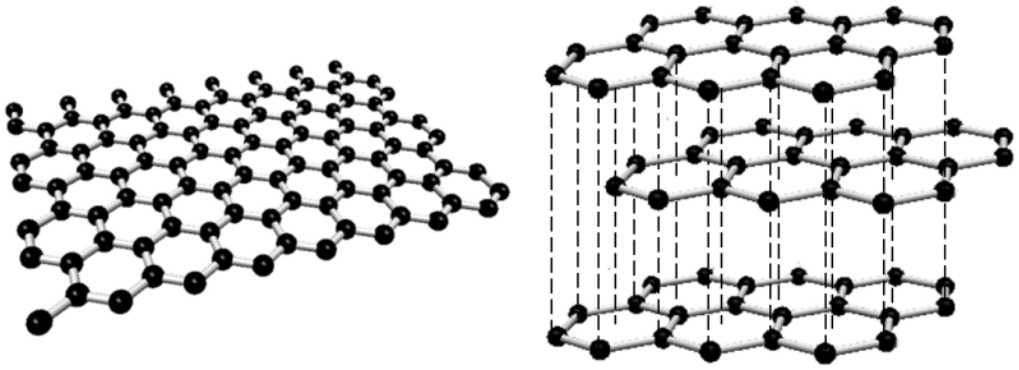

Figure 1.7: 2D honeycomb structure of graphene (left) and stacked graphene layers forming bulk graphite (right) [19].

fermions [21]. Being an atomically-thin material with attractive electrical properties, graphene has been widely considered for and tested in applications involving nano-electronics.

This so-called wonder material, alongside its electrical properties, also has very impressive mechanical characteristics [22]. In particular, graphene has been found to have an out-of-plane Young's modulus (E) value of $\sim$1 TPa and a tensile strength of $\sim$130 GPa, which were measured by AFM-based nano-indentation experiments performed on graphene membranes suspended over micron-sized circular holes etched on SiO_2 [22].

As one can see, the combination of outstanding electrical and mechanical properties (in addition to unexpected optical and thermal attributes not mentioned here) make graphene truly a wonder material for various applications, including but not limited to the field of micro-/nano-electromechanical devices.

1.3.2 Graphene as a Lubricant

As it was quickly found out after its discovery that graphene exhibited outstanding mechanical strength and electrical properties, it was not long before several research groups turned their attention to its frictional characteristics [23-31]. These

efforts were greatly motivated by the fact that bulk graphite (which essentially consists of stacked layers of graphene) has long been used as a lubricant –either by itself as a *solid lubricant*, or as an additive for oil-based lubricants– for mechanical devices and processes [32, 33]. While a major problem with the use of bulk graphite as a solid lubricant is the fact that it requires a humid environment to function well [33], graphene has been recently found to not suffer from such a limitation [23]. Combined with the fact that graphene also provides extensive corrosion and oxidation resistance to the surfaces that it covers [34], the potential use of graphene as a solid, atomically-thin lubricating layer becomes even more intriguing.

The application of graphene as a solid lubricant is especially attractive for micro-/nano-electromechanical devices where high surface-to-volume ratios increase the influence of surface phenomena such as friction and wear on device operation, and excessive surface tension prevents the use of conventional, liquid-based lubrication schemes. While a particular study in the literature was able to demonstrate frictional behavior that strongly depends on the number of layers for mechanically-exfoliated graphene samples (explained by a so-called *puckering* mechanism) [26], the precise role that interface structure (both in terms of size and roughness) plays in the lubricative properties of graphene has not been explored in detail yet. Taking into account that this is an important design parameter for mobile components featured in micro-/nano-electromechanical devices, we present in this thesis a detailed investigation of the nanotribological characteristics of graphene as a function of interface structure. Overall, we are of the opinion that the results discussed here help pave the way toward the practical utilization of graphene-based solid lubrication schemes in micro- and nano-scale systems.

1.4 Outline

This thesis is divided into five separate chapters.

The current chapter (Chapter 1) presents an overview of the field of tribology, its sub-discipline nanotribology, and the operational details of contact-mode atomic force microscopy and friction force measurements. The chapter concludes with a brief discussion of the physical properties of graphene and in particular, its nanotribological characteristics.

Chapter 2 contains technical details associated with the preparation and structural characterization of graphene samples. The method of mechanical exfoliation is introduced and characterization experiments performed via optical microscopy, Raman spectroscopy and topographical AFM imaging are exemplified.

Chapter 3 deals with AFM tip calibration and modification. Conventional techniques employed for the calibration of AFM tips for accurate detection of normal and lateral forces are discussed. Additionally, various methods utilized for tip modification, including but not limited to thermal evaporation of noble metals onto tip apexes, are introduced.

Chapter 4 comprises a detailed discussion of the nanotribological properties of mechanically-exfoliated graphene; as a function of applied normal load, number of layers, tip size and interface roughness. The presented experimental results are complemented by molecular dynamics (MD) simulations performed in collaboration with the research group of Prof. Ashlie Martini at the University of California, Merced (UC Merced).

Chapter 5 finally provides a summary of the thesis and an outlook regarding future directions of research.

Chapter 2

Preparation and Characterization of Samples

2.1 SiO_2 Substrate Preparation

For ease of structural identification based on conventional techniques reported in the literature [16], the preferred substrate to transfer exfoliated graphene onto was chosen as silicon wafers covered with a thin (300 nm) layer of silicon dioxide (Si/SiO_2). Although highly transparent, graphene can be optically identified when it is situated on such substrates.

In order to increase the number of graphene flakes successfully transferred onto Si/SiO_2, the substrates must be as clean as possible. To achieve this goal, Si/SiO_2 wafers were subjected to a cleaning procedure. 3-inch wafers were unpacked in the National Nanotechnology Research Center (UNAM) cleanroom, and then were diced into 10 mm $\times$ 10 mm pieces using the dicing saw. The diced wafers were then ultrasonically cleaned in acetone, isopropyl alcohol, and distilled water, respectively. Any remaining moisture on the surfaces was expelled using a dry nitrogen gun.

An alternative method utilized to clean the diced Si/SiO_2 wafer pieces involved the use of the *piranha solution*, which is a highly corrosive substance used for removing organic contamination. The solution is prepared by mixing 1-part hydrogen peroxide (H_2O_2) into 3-parts sulfuric acid (H_2SO_4) very slowly [35]. Piranha solution is then poured directly into a Teflon container containing the diced Si/SiO_2 wafer pieces to be cleaned.

Based on our observations, neither of the two cleaning procedures described here provided a comparatively higher rate of transfer of exfoliated graphene onto Si/SiO_2. As such, the ultrasonic cleaning method was preferred for all following experiments, as it is safer to utilize.

2.2 Mechanical Exfoliation of Graphene

Graphite is one of the allotropes of carbon, which consists of multiple graphene layers stacked on top of each other. To obtain pristine graphene, a source of bulk graphite needs to be mechanically cleaved or in other words, exfoliated. Three different forms of bulk graphite were used as source material for graphene in our experiments: A-quality-level Highly Ordered Pyrolytic Graphite (HOPG), B-quality-level HOPG, and graphite flakes (Figure 2.1). When the results of exfoliation experiments were compared, it was determined that none of these bulk sources yielded a comparatively higher transfer rate for graphene. Therefore graphite flakes were utilized for all further experiments, as it is inexpensive compared to HOPG.

To perform mechanical exfoliation, the source of bulk graphite is placed on the adhesive side of a Scotch Tape, the tape is firmly pressed on the source, and then slowly peeled away. The graphitic structure remaining on the adhesive tape is still bulk graphite; by folding the adhesive tape onto itself, compressing it, and peeling away slowly, the number of layers associated with the graphite is decreased. This step is repeated until a barely-visible layer of graphite is left on the adhesive tape. This thin layer of graphite is then pressed onto the previously cleaned

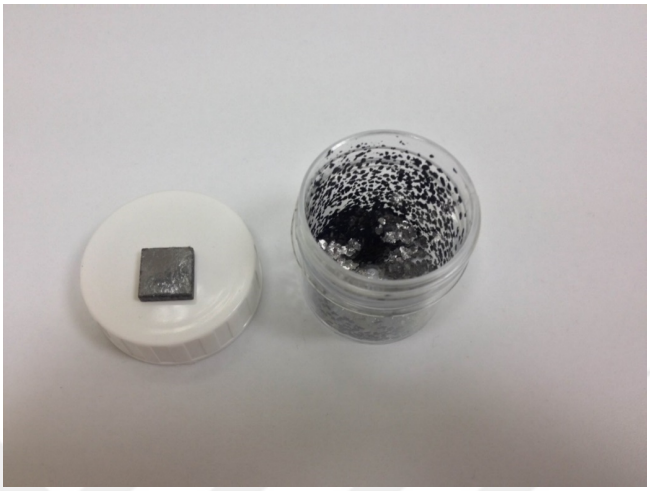

Figure 2.1: A 1 cm × 1 cm HOPG sample (left), and graphite flakes (right).

Si/SiO_2 substrate and peeled away, leaving behind (in most cases) multiple few- and single-layer graphene flakes.

As discussed in Chapter 1, different layers of graphene in bulk graphite are held together only by weak van der Waals interactions [36]. Consequently, when pressed against a SiO_2 surface, adhesion between SiO_2 and graphene layers is typically enough to cleave single- and few-layers of graphene away from graphite and transfer it onto the SiO_2 surface.

2.3 Optical Microscopy

The first step for identifying graphene flakes on Si/SiO_2 substrates involves conventional optical microscopy. Although single- and few-layer graphene is transparent under visible light, it has been shown that Si wafers covered with ∼300-nm-thick SiO_2 provide an increased optical path, shifting interference colors and thus making graphene optically detectable [16].

Under the optical microscope used during our experiments (*Keyence VK-X100*), the Si/SiO_2 substrate appears purple-colored. On the other hand, single-layer graphene, which is highly transparent, appears as a darker shade of purple

(Figure 2.2). As the number of layers increases, the color shifts further to blue (for few layers of graphene), and finally approaches white (for bulk graphite).

During our experiments, it was possible to find single-layer graphene flakes that are as big as 20 μm $\times$ 20 μm laterally. However, in order to be able to investigate the effect of number of layers of graphene on friction via atomic force microscopy, specific flakes with "stair-like" structures exhibiting 1-2-3-4 layers of graphene were required. During our investigations, it was observed that these structures were often found next to bulk graphite pieces, unlike large single-layer graphene flakes that were situated mostly in a stand-alone fashion on the Si/SiO_2 substrates.

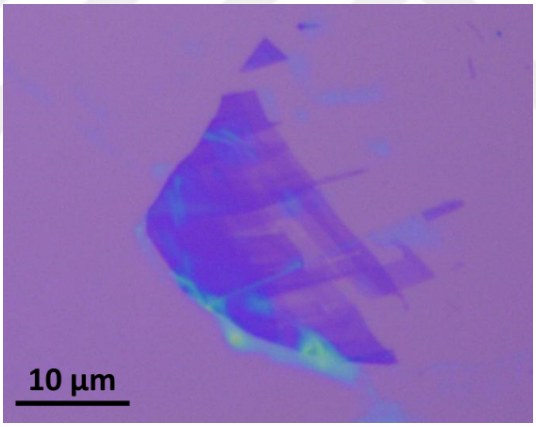

Figure 2.2: Optical microscopy image of a SiO_2 region with few- and multi-layer graphene on top.

2.4 Raman Spectroscopy

Raman spectroscopy, named after and invented by Sir Chandrasekhara Venkata Raman (1888-1970) in year 1928, is an analytical characterization method which utilizes the inelastic scattering of light to chemically identify materials [37]. The basic principle of operation (Figure 2.3) involves the sample to be chemically identified being illuminated by monochromatic (i.e., constant-wavelength) light from a laser source. Most of the photons of the incoming laser interacting with the sample are scattered elastically (i.e., no change in photon energy). This is

named as Rayleigh scattering, and these photons are filtered out in the Raman spectrometer. On the other hand, the remaining minority of photons lose or gain energy when scattering after reaching the sample, due to interactions with sample phonons. This is called Raman scattering, and by detecting and analyzing the differences in energy between these inelastically scattered photons and the incoming photons of the monochromatic laser beam, it is possible to chemically differentiate and identify sample materials, since all materials exhibit characteristic Raman scattering spectra [38].

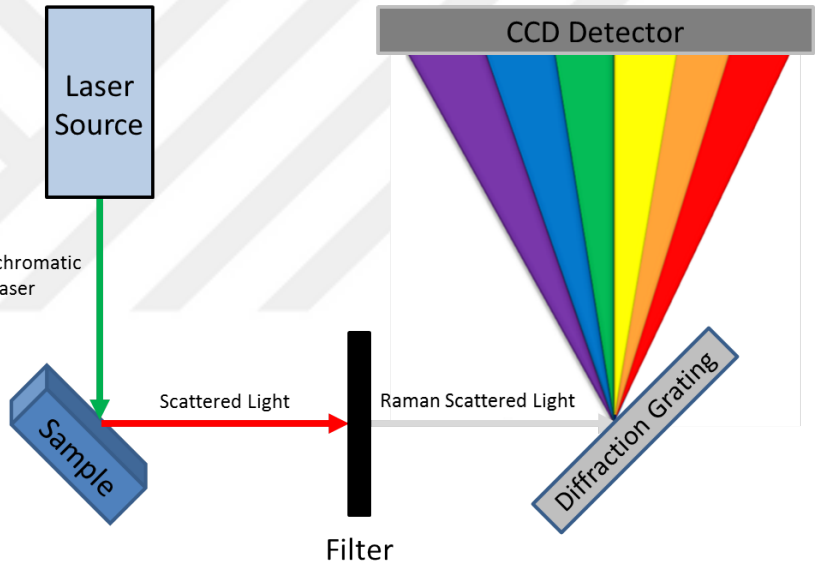

Figure 2.3: Illustration of the main components of a Raman spectrometer.

After the discovery of graphene via mechanical exfoliation [16], Raman spectroscopy was one of the first analytical methods that have been employed for its characterization. In particular, it has been shown that the number of layers of graphene can be precisely identified with Raman spectroscopy [39].

Specifically, there are three main peaks in the Raman spectrum of graphene: **(i)** A D-peak positioned at a *Raman shift* of 1350 cm^{-1}, which is related to structural defects of the graphene sample (lower peak intensity for less defects, see Figure 2.4 for a representative spectrum of nearly defect-free graphene), and then, **(ii)** a G-peak positioned at 1580 cm^{-1}, and **(iii)** a 2D-peak positioned at 2680 cm^{-1}, which are related to the graphitic (i.e., carbon-related) properties of

the sample. If the relative intensity ratio of the 2D-peak to the G-peak (I_{2D}/I_G) is equal to or higher than 2, the sample is considered to be single-layer graphene; if I_{2D}/I_G is approximately 1, the sample is 2-layer graphene; and if it is less than 1, the sample is multi-layer graphene (HOPG-like). Reference Raman spectra for single-layer graphene and bulk graphite are provided in Figure 2.4 [39].

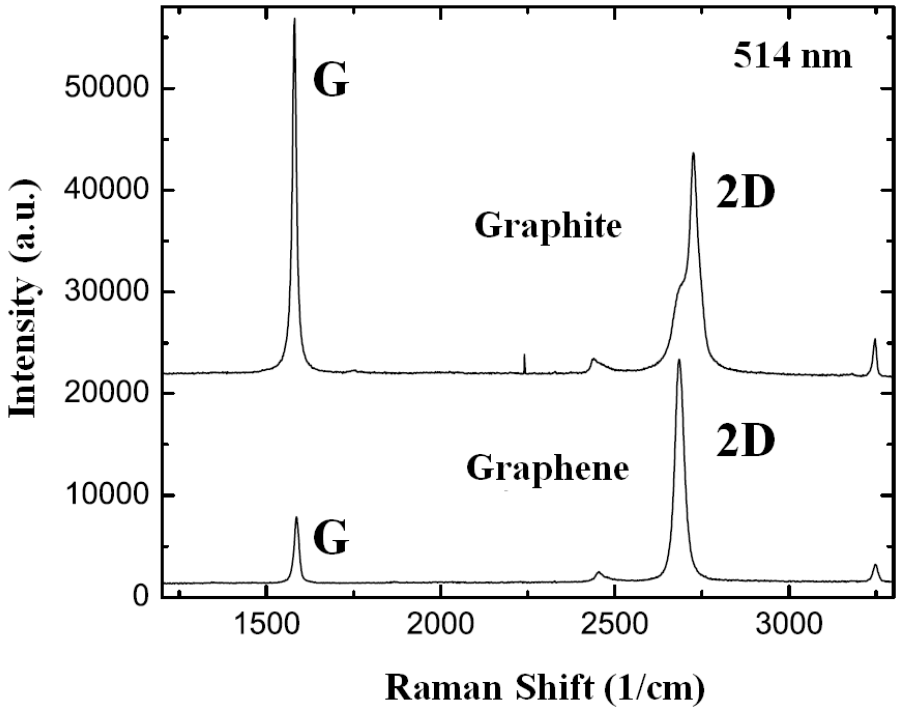

Figure 2.4: Raman spectra of graphite and exfoliated graphene measured using a 514 nm wavelength monochromatic laser [39].

A second step of confirmation regarding the single-layer character of graphene based on its Raman spectrum involves the shape of the 2D-peak. For a single-layer graphene sample, the 2D-peak must fit a Lorentzian function showing that there are no secondary peaks, which would be indicative of the sample being multi-layer (HOPG-like), as seen in Figure 2.4. The specific full width at half maximum (FWHM) value of this Lorentzian function is also an indication of single-layer graphene [40]. Figure 2.5 shows the Raman spectroscopy data that we have acquired on a single-layer graphene flake using the *WITec alpha300 RAS* Raman spectrometer available in UNAM, together with a Lorentzian fit. As expected, the data exhibit no secondary peaks, and the FWHM value of $\sim$36 cm^{-1} is indicative of single layer character [40]. Throughout the experiments described

in this thesis, using Raman spectroscopy, we were able to successfully identify single-, bi-, and multi-layer exfoliated graphene samples on Si/SiO_2 substrates.

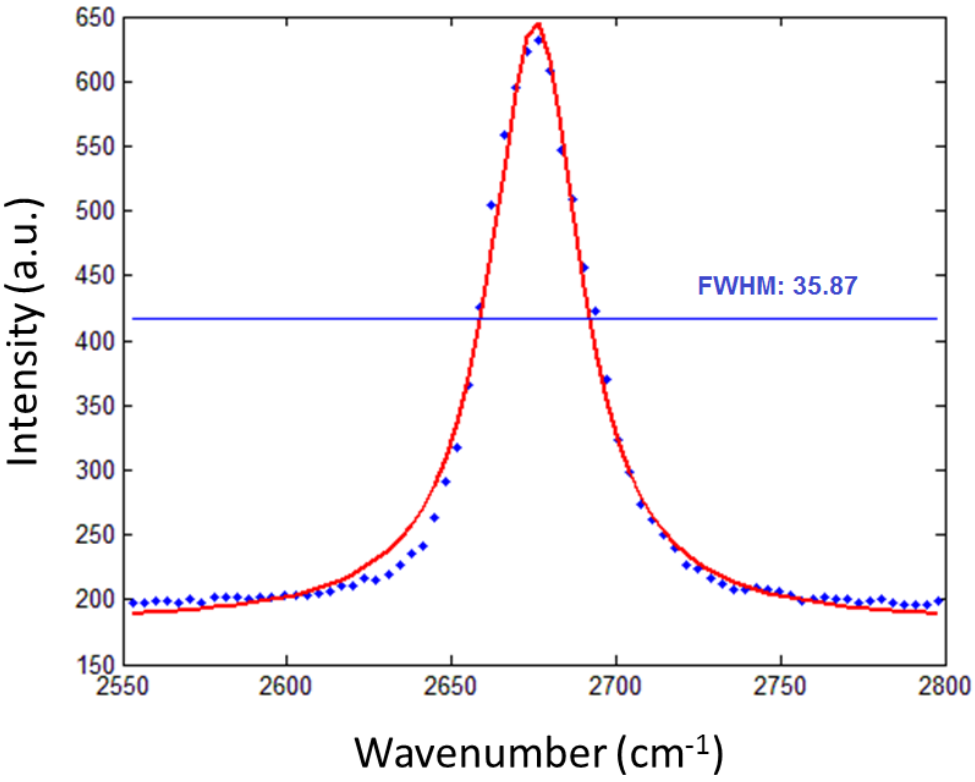

Figure 2.5: Lorentzian fit applied on a set of data points for a 2D-peak associated with the Raman spectrum of a single-layer graphene sample. The full width at half maximum (FWHM) value of $\sim$36 cm^{-1} is indicative of single-layer character.

2.5 Topographical AFM Measurements

Using Raman spectroscopy, it is not possible to differentiate the number of layers of graphene in regions with more than 2 layers. For instance, Raman spectroscopy is not able to provide data that would allow researchers to reliably identify and separate regions exhibiting 3- and 4-layer graphene. Moreover, being a spectroscopic technique based on spatial averaging of data, Raman spectroscopy does not provide real-space, high-resolution (i.e., nanometer-scale) information on the structure of graphene samples. Based on these reasons (in order to determine the

number of layers in multi-layer graphene regions and to visualize with high resolution the associated topography), AFM has been utilized in our experiments. Specifically, we have employed a commercial AFM instrument available at UNAM for our research (*PSIA XE-100*, see Figure 2.6).

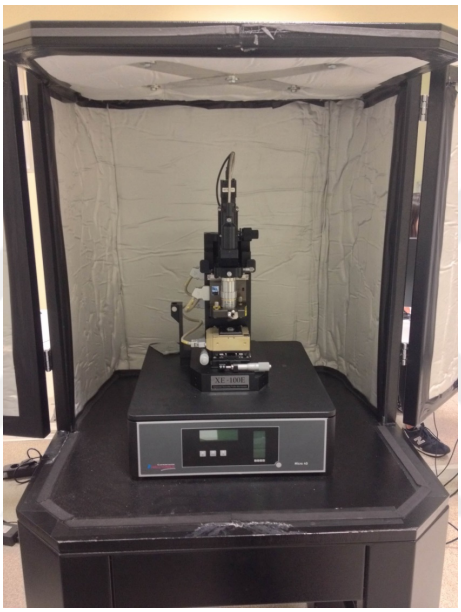

Figure 2.6: The AFM instrument used for the experiments presented in this work.

As already described in Section 1.2.1, AFM is routinely used to map various sample surfaces topographically with sub-nm resolution. As such, AFM can also be used to determine the number of layers associated with a multi-layer graphene sample by measuring the height differences relative to a known 1- or 2-layer graphene region, which was, for instance, previously identified by Raman spectroscopy. The distance between individual layers of single-atom-thick graphene is expected to be ∼3.4 Å [16]. However, when mechanically-exfoliated graphene is transferred onto a Si/SiO_2 substrate, due to trapped air and moisture between the substrate and graphene, the height of the initial graphene sheet above the substrate is quite variable (up to ∼1.5 nm; see, e.g., Figure 2.7) [16]. Therefore, in order to be able to identify 3 or more layers of graphene, the height difference must not be measured from the base substrate, but instead, from a previously identified 1- or 2-layer graphene region, due to the variability of the height of the first layer that adheres to the Si/SiO_2 substrate. In particular,

Figure 2.8 demonstrates the topographical AFM image associated with a "stair-like" graphene flake and the assigned number of layers based on height variations measured by AFM. It should also be mentioned that AFM allows the detailed visualization of structural features associated with graphene samples, for instance the above-mentioned pockets of trapped air/moisture, as well as possible micro-scale contaminants left on the graphene surface due to the application of the adhesive tape during the transfer process.

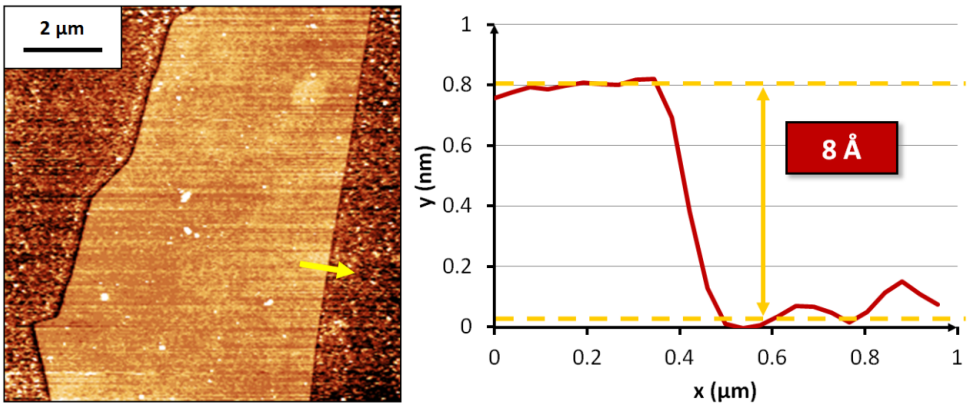

Figure 2.7: Topographical map of a single-layer graphene flake (left) and the profile of the yellow line showing the height of single-layer graphene above the Si/SiO_2 substrate as ~8 Å (right).

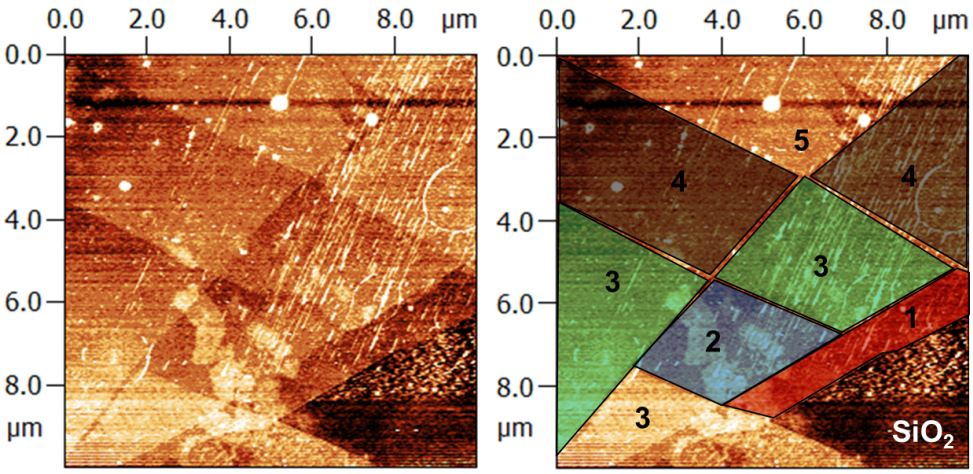

Figure 2.8: Topographical AFM image of a region comprising the Si/SiO_2 substrate and a stair-like flake with 1, 2, 3, 4 layers of graphene. Micro-scale contaminants and pockets of trapped air/moisture can also be observed.

Chapter 3

AFM Tip Calibration and Characterization

3.1 Sader's Method (k)

Contact-mode atomic force microscopy enables us to precisely measure normal and lateral forces experienced by the AFM probe when scanning over a given sample surface. During an individual scan, the AFM instrument measures the deflection of the cantilever in the vertical z direction and the topographical feedback system adjusts the z-scanner height in order to keep the normal (i.e., vertical) load value applied by the cantilever to the sample constant throughout the whole scan. As the normal load is simply the product of cantilever deflection and its normal spring constant (k), k values for individual cantilevers need to be precisely determined and entered into the AFM software for accurate normal load readings.

The normal spring constant of the cantilevers used in this work are determined by the method developed by Sader *et al.* [41],whereby the associated calibration is based on measuring the resonance frequency of the cantilever:

$$k = M_e \, b \, h \, L \, \rho_c \, {w_{vac}}^2 \tag{3.1}$$

where M_e is the normalized effective mass of the cantilever, typically taken as 0.2427 (as determined by the aspect ratio of the cantilever [41]), b, h, L are the width, thickness and length of the cantilever (50 μm, 2 μm, 450 μm, respectively [42, 43]), ρ_c is the density of the material out of which the cantilever is made (taken as 2.329 g/cm^3 for Si), and w_{vac} is the angular resonance frequency of the cantilever in vacuum. For our experiments, the resonance frequency of the cantilever is measured under ambient conditions. Therefore, before applying Eq. (3.1) to calculate k, a $\sim$2% decrease in w_{vac} under ambient conditions is taken into account due to air damping [41].

Cantilevers used throughout this thesis are commercially available, conventional contact-mode probes produced by *BudgetSensors* and *NanoSensors* (models *ContAl-G* and *PPP-CONTR*, respectively, see Figure 3.1). The normal spring constant values calculated for the cantilevers vary between 0.13 N/m and 0.24 N/m, which is within the range of the values provided by the manufacturers and close to the nominal value of 0.20 N/m [42, 43].

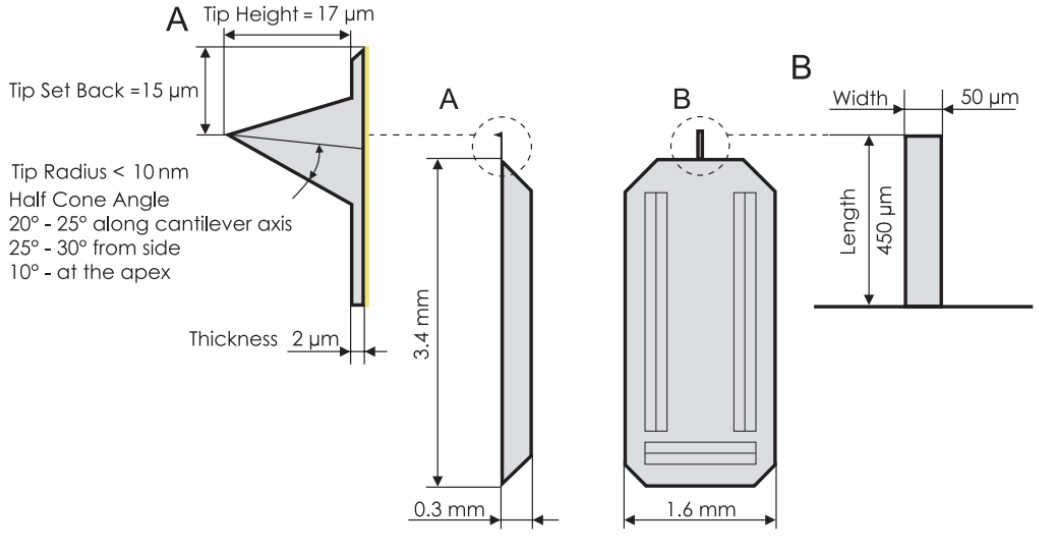

Figure 3.1: Schematic drawing detailing the dimensions of a *BudgetSensors* *ContAl-G* AFM cantilever [43].

3.2 Ogletree's Method (α)

Calculating the normal spring constant of a cantilever as described in Section 3.1 allows the AFM software to utilize accurate normal load values during scanning. On the other hand, for accurate measurements of nanoscale friction, different AFM cantilevers must also be calibrated for lateral force measurements. The AFM instrument measures the lateral forces experienced by the probe (resulting in the *twisting* of the cantilever) as voltage readings arising from the lateral displacements of the laser spot on the PSPD. As such, a lateral calibration constant (α) needs to be calculated to accurately convert the voltage readings to lateral force values.

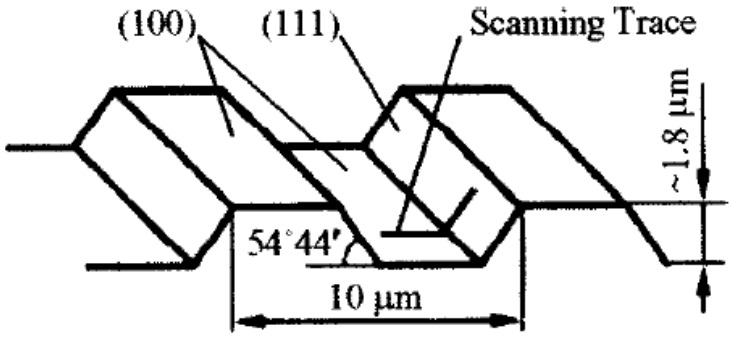

Figure 3.2: Schematic drawing of the *MikroMasch TGF11* silicon calibration grating which was employed to calibrate lateral force readings for all cantilevers used in this work [45].

In order to determine α values for each cantilever used in the experiments described in this thesis, the traditional method introduced by Ogletree *et al.* [44] has been utilized, in conjunction with a commercial calibration grating (*TGF11* by *MikroMasch*, see Figure 3.2), as suggested by Varenberg *et al.* [45]. In particular, the calibration grating featuring pre-defined slopes with known angles ($\theta \approx 54°$) is scanned by the AFM probe for which the α value needs to be determined, at varying values of normal load. The voltage readings corresponding to lateral forces experienced by the cantilever are recorded on the sloped regions of the grating for each value of the normal load, and for both forward and backward scans that together form *friction loops* (see Section 1.2.2). Subsequently, friction loop half width (W) and friction loop offset (D) values are determined. These values

are plotted against increasing normal load. The slopes of these plots (W', D') are then put into the following equations arising from force equilibrium arguments [44]:

$$\alpha \times D' = \frac{(1+\mu^2)\sin\theta\cos\theta}{(\cos\theta)^2 - \mu^2(\sin\theta)^2} \tag{3.2}$$

$$\alpha \times W' = \frac{\mu}{(\cos\theta)^2 - \mu^2(\sin\theta)^2} \tag{3.3}$$

Finally, Equations (3.2) and (3.3) are solved simultaneously for the two unknowns: the lateral force calibration constant α, and the coefficient of friction μ. The lateral force calibration constant values calculated in this way for the cantilevers used in this thesis vary between 5.1 nN/V and 19.6 nN/V.

3.3 SEM Imaging of AFM Probes

As one of the principle aims of this thesis is to investigate the frictional properties of graphene as a function of contact size, structural characterization of AFM probes is an important pre-requisite for physical insight. While optical microscopy is limited in spatial resolution due to the relatively large wavelengths associated with the visible light spectrum, and thus cannot be used for this goal, SEM utilizes high-energy (on the order of keV) electrons to provide imaging capabilities with much higher resolution (often down to ∼10 nm or below). Consequently, in order to be able to image AFM probes with radii of curvature as small as 10 nm, SEM has been utilized in this work.

The basic operating principle of SEM can be summarized as follows (see Figure 3.3): Electrons are emitted from an electron gun and are accelerated by a positively-charged plate. This high-energy electron beam is then focused onto the sample surface via magnetic lenses. Electrons interacting with the sample surface are scattered either elastically (*backscattered* electrons) or inelastically (*secondary*

electrons) and are collected by dedicated detectors. While backscattered electrons provide high-spatial-resolution information about the chemical composition of the sample surface, topographical structure of surfaces is reproduced with high resolution by collecting secondary electrons and subsequent conversion to a 2D image via a process called *cathodoluminescence* [46].

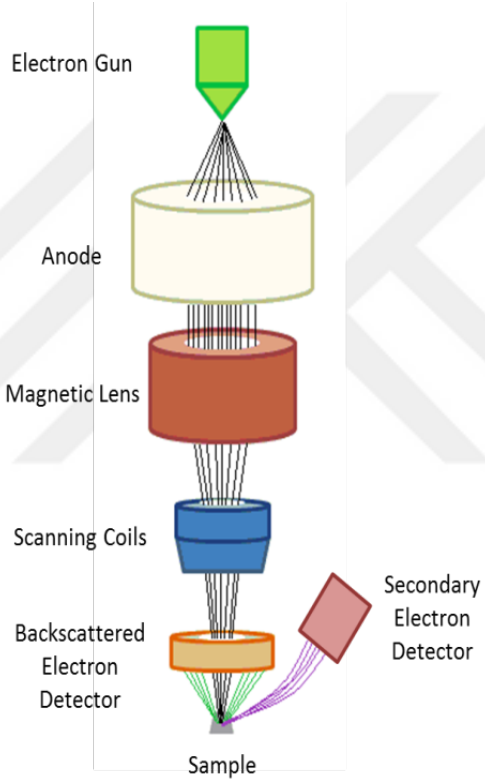

Figure 3.3: Illustration of the main components of a scanning electron microscope.

Within the context of the experiments reported in this thesis, before every topographical/frictional measurement, AFM probes were characterized structurally via SEM to measure the respective tip apex diameter and to make sure that there are no major defects associated with the probe (such as attached particles or a fracture). Figure 3.4 demonstrates such a measurement, where an AFM probe with an apex diameter of ∼25 nm has been imaged in SEM. The environmental SEM (*FEI Quanta 200*) available at UNAM was used for all SEM measurements.

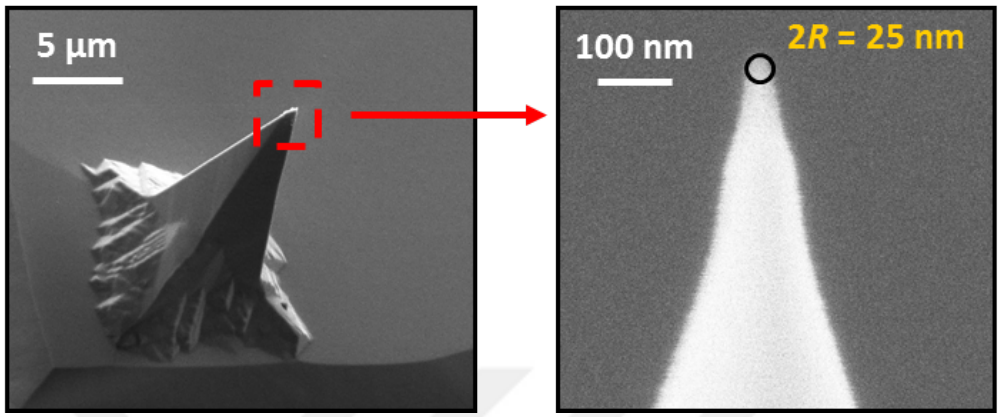

Figure 3.4: Large- and small-scale SEM images of an AFM probe with an apex diameter of ∼25 nm.

3.4 Tip Modification

Nanoscale frictional behavior is expected to depend on the structure of the interface (both its size and roughness) as well as the material properties associated with the two surfaces that are sliding against each other [12]. Therefore, to investigate the effect of interface structure and materials on the frictional behavior of graphene, AFM probe tips were modified in this thesis using various coating methods, which allowed changing the material, size and the roughness of the probe tip. Different methods of AFM probe tip modification will be illustrated in this section.

3.4.1 Carbon Coating

During electron-beam-based imaging of AFM probes, even minimal amounts of carbon-based contaminant molecules inside the vacuum chamber can be deposited onto the probe surfaces due to the presence of the high-energy electron beam, which catalyzes the deposition process [47]. The coating forming on the tip surface is an amorphous hydrocarbon layer, the growth of which can be tracked *in-situ* while imaging the probe in the SEM instrument. This fact provides an opportunity for *controlled* growth and probe apex size modification, as the carbon

deposition can be simply stopped by turning off the electron beam. Figure 3.5 demonstrates the controlled modification of an AFM probe tip via this procedure.

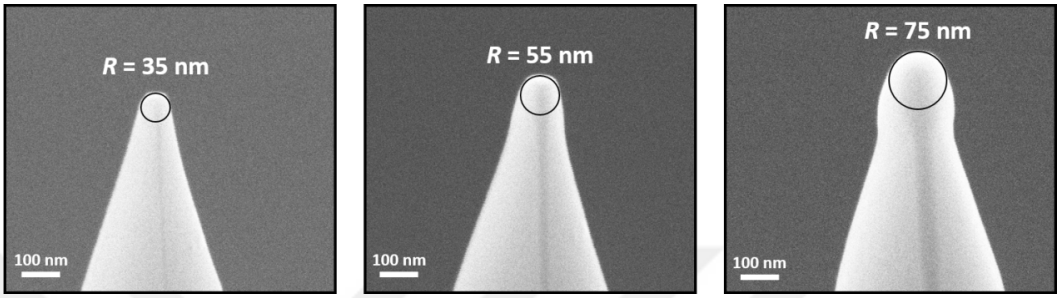

Figure 3.5: An AFM probe tip coated with a carbon layer up to a tip radius of ∼35 nm inside the SEM instrument (left), and the same tip coated more to reach tip radii of ∼55 nm (center) and ∼75 nm (right).

Although the carbon coating process is very controllable in terms of adjusting probe apex growth, the nanoscale friction results obtained with AFM probes modified in this fashion were not highly reproducible, especially when compared to metal-coated probes (see below). We tentatively attribute this observation to the fact that hydrocarbon-based coatings on the AFM probes are expected to be *softer* (i.e., mechanically weaker) than metal-based coatings, which yielded more consistent results. Therefore, nanoscale friction experiments reported in this thesis (see Chapter 4) have all been performed using metal-coated AFM probes.

3.4.2 Gold Coating

Gold was the first metal chosen to be coated on our AFM probes. It was selected because gold is commonly known as the most non-reactive (i.e., noble) metal [48], which allows gold-coated probes to be used, in principle, without any chemical degradation under ambient conditions over extended periods of time. Another, perhaps more practical, reason for the use of gold as a coating material for our AFM probes was the fact that it was readily available in our research group, and the instrumental parameters associated with precision etching coating system (PECS)- or thermal-evaporation-based coating of gold were already known.

Gold coating of AFM probes has been achieved in two different ways:

I. The PECS instrument (by *Gatan*) available at UNAM which is typically utilized for gold-coating of non-conducting SEM samples has also been found useful for gold-coating of AFM probes. In particular, PECS utilizes ion guns to sputter a thin coating layer onto the sample from a target material, such as gold. Using the PECS instrument, AFM probes were sputtered with gold to uniformly increase tip diameters to pre-determined values before friction measurements.

II. Alternatively, thermal evaporation can be employed to coat AFM probes with gold. The working principle of a conventional thermal evaporator is as follows (see Figure 3.6): The material to be evaporated and coated onto the substrate is placed inside a "boat" (made mostly out of tantalum or tungsten) through which electrical current flows. The sample that will be coated is placed above the boat, facing it. The whole setup is housed inside a vacuum chamber that can reach base pressures on the order of 10^{-6} mbar. By providing current through the boat, the material is heated up and starts to evaporate. The evaporated material moves toward the sample and adsorbs upon contact with the substrate, thus coating it. The commercial thermal evaporation instrument available at the UNAM cleanroom (*Vaksis MiDAS PVD 3T*) has been successfully utilized in the present thesis to modify AFM probes via gold-coating (Figure 3.7).

It was found during our experiments that PECS and thermal evaporation methods do not pose significant advantages with respect to each other in terms of tip modification. As equipment malfunction for both instruments was a common issue, the two methods were used interchangingly throughout the thesis work.

3.4.3 Platinum Coating

In order to be able to compare and evaluate the effect of using different probe materials on the frictional behavior of graphene, some probes were coated with platinum (instead of gold) using the PECS system. Remarkably, the use of

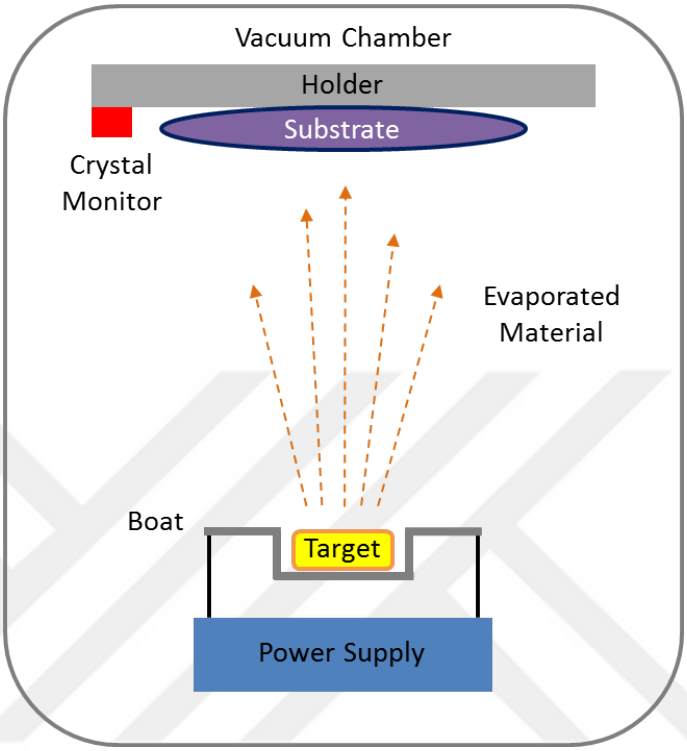

Figure 3.6: Schematic drawing of the main components of a thermal evaporator.

platinum-coated AFM probes yielded unexpected trends in the friction experiments, involving in most cases the observation of *decreasing friction* values with *increasing normal load*, pointing to a "*negative coefficient of friction*". While this phenomenon was previously reported for AFM-based friction experiments performed on bulk graphite, and explained by a mechanism that involves adhesion of the top layer of graphite onto the AFM probes [49], our observations are too preliminary to draw parallels to these experiments. On the other hand, the fact that the surface energy of platinum (2.48 J/m^2) is considerably higher than the surface energy of gold (1.50 J/m^2) [50] might help explain the related observations with an adhesion-based mechanism. This should, nevertheless, be the subject of future work.

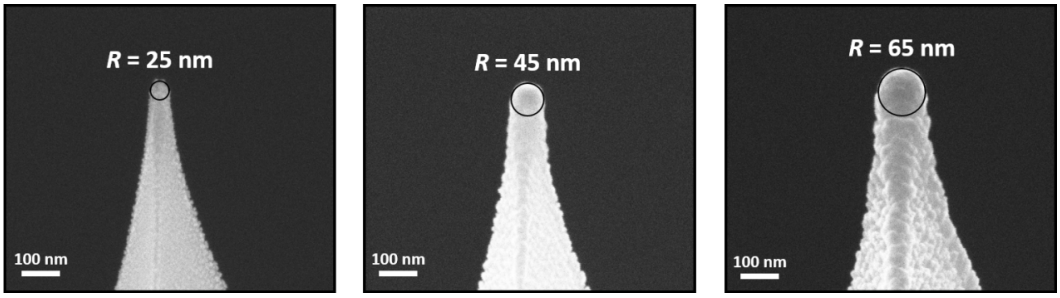

Figure 3.7: An AFM probe tip coated with gold up to a tip radius of ∼25 nm (left), and the same tip coated more to reach tip radii of ∼45 nm (center) and ∼65 nm (right).

3.4.4 Adjusting Calibration Parameters After Tip Modification

While performing tip modification via coating with PECS or thermal evaporation, it is not possible to coat the apex by itself without affecting the whole cantilever. As such, during tip modification, AFM cantilevers are coated as well and their dimensions change. Therefore, k and α values have to be adjusted after every modification to compensate for the structural changes in the cantilevers.

The cantilevers used in this work are made of silicon. As already discussed, not only the tip gets covered with a layer of metal during modification, but also the bottom side of the whole cantilever. Therefore an effective Young's modulus (E_e) for the silicon/metal cantilever system needs to be calculated to be able to obtain an adjusted spring constant k for the coated cantilever [41]:

$$E_e = \frac{E_{coating}h_{coating} + E_{cantilever}h_{cantilever}}{h_{coating} + h_{cantilever}} \tag{3.4}$$

where E is Young's modulus and h is the thickness of the elements indicated by the subscripts.

Using the effective Young's modulus value, Sader *et al.* approximated the coated cantilever's spring constant as [41]:

$$k_{coated} = k_{uncoated}\left(\frac{h_{coating} + h_{cantilever}}{h_{cantilever}}\right)^3 \frac{E_e}{E_{cantilever}} \tag{3.5}$$

where k is the spring constant, h is the thickness and E is the Young's modulus of the elements indicated by the subscripts. After every coating process, the spring constant of the cantilever was updated manually in the AFM software to accurately perform normal load readings.

It should be indicated that the spring constant adjustment for modified cantilevers is only performed for the metal-coated ones, as carbon-coating inside the SEM only occurs at the tip of the probe where the high-energy electron beam is focused. In other words, the body of the cantilever is not coated by carbon during this process.

For lateral force calibration, it should be taken into account that when the cantilever body is coated, the thickness of the cantilever (h) also increases, resulting in an increase in the polar moment of inertia (J) of the cantilever beam which is proportional to bh^3 (b is the width and h is the thickness of the cantilever). This change in polar moment of inertia affects the torsional angle of twist (θ) caused by the lateral forces acting on the tip apex:

$$\theta = \frac{T\ l}{G\ J} \tag{3.6}$$

where l is the length and G is the shear modulus of the cantilever. Additionally, T is the applied torque on the cantilever, which is directly proportional to the lateral forces acting on the tip apex. Therefore, for any change in the thickness (h) of the cantilever, the angle of twist in response to an applied lateral force (or consequently, T) needs to be calculated for pre- and post-coating thicknesses. The ratio of pre-coating angle of twist to post-coating angle of twist ($\theta_{before}/\theta_{after}$) is then multiplied with the lateral force calibration constant to compensate for the modification in the thickness of the cantilever.

Chapter 4

Nanotribology of Exfoliated Graphene

4.1 Effect of Applied Load

As a starting point for investigating the tribological properties of graphene at the nanoscale, the effect of applied (i.e., normal) load on friction was quantified with numerous AFM measurements. To make sure that the only independent variable to be investigated is the applied load in these experiments, lateral force measurements were performed on relatively large (with lateral dimensions above 10 μm) single-layer graphene flakes, eliminating the effect of layer-dependence of friction on graphene.

During the experiments, it was observed that graphene flakes would often be ripped apart and folded at applied load values around 30 nN (see, for instance, Figure 4.1). As such, the absolute maximum applied load value for friction experiments on graphene was chosen as 22 nN, to prevent structural modification of graphene flakes by the AFM probes. The starting applied load value for the measurements is taken as 0 nN, which is incrementally increased by 2 nN after each scan of the same region to reach the maximum applied load value of 22 nN,

resulting in a total of 12 data points of friction for every set of measurements to be evaluated quantitatively. It must be mentioned that due to the existence of finite adhesion between the AFM probe and the sample surface, an applied load of 0 nN results in an effectively non-zero normal force interaction (see Section 4.3). For flakes that were more prone to be structurally manipulated/damaged, the incremental increase of applied load was restricted to 0.5 nN steps and an upper limit of 5.5 nN.

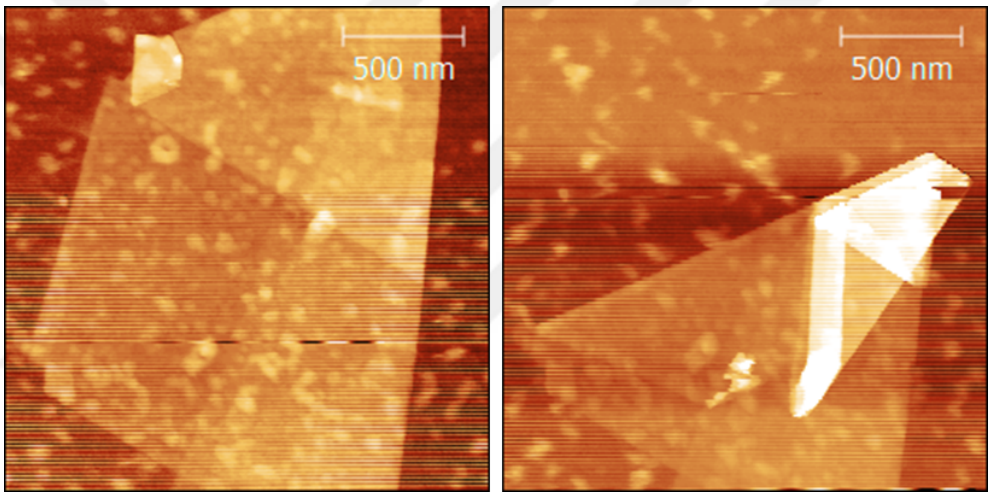

Figure 4.1: Topographical images of a graphene flake with single-/multi-layered regions (left), and the same flake folded over itself multiple times (right). The applied load was 25 nN for this measurement.

Previous experimental studies in literature have shown that the friction force values measured on exfoliated graphene increase –as one would intuitively expect– with increasing applied load [29, 51]. These findings were also confirmed by molecular dynamics (MD) simulations [52]. The results obtained in this work confirm the qualitative statements in the literature regarding the monotonous increase of friction with increasing applied load. Furthermore, the relation between friction force and applied load has been also quantitatively analyzed in our work. In particular, it was found that the dependence of friction on applied load can be described equally well by a linear fit (as expected from Amontons' law of macroscopic friction) and a Hertzian description (relevant for a *single-asperity* geometry):

$$F_f = A\,(F_n + B)^{2/3} \tag{4.1}$$

where F_f is the friction force, F_n is the applied load, A is a simplified parameter related to the geometric and material properties of the slider (AFM probe) and the substrate (graphene) such as apex radius and Young's moduli, and B is an offset term that describes the tip-sample adhesion force. The R^2 values of linear and Hertzian fits on multiple measurement data on single-layer graphene were compared to see which model was more suitable for the acquired data (see, e.g., Figure 4.2). As one can see, the differences in R^2 values obtained via linear and Hertzian fits were always found to be rather insignificant and as such, it is not possible to make a definitive remark on which model fits the frictional behavior of graphene better. It is projected that in order to make a better comparison, a larger range of applied load values should be employed (which, on the other hand, might lead to structural/morphological damage of graphene flakes, as discussed earlier).

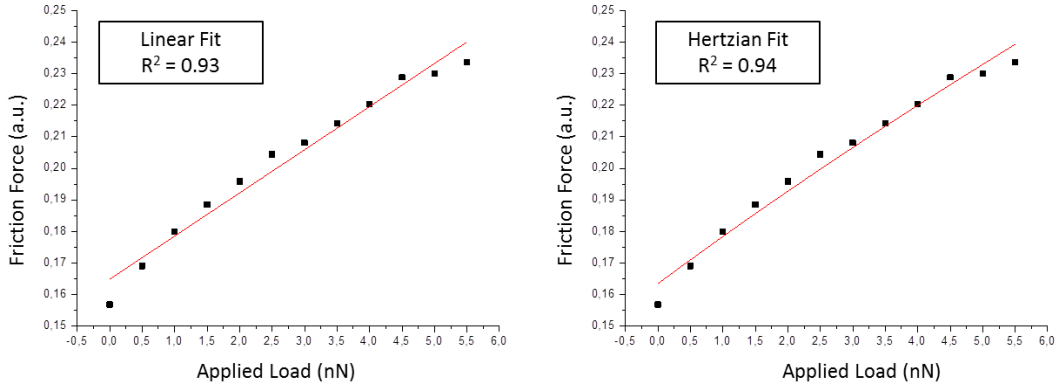

Figure 4.2: Linear and Hertzian fits applied on the same data set of friction force vs. applied load, showing very similar R^2 values for the two approaches.

Before concluding this section another remark should be made: During these initial experiments regarding the effect of applied load on measured friction, it has been observed that the height of single-layer graphene flakes decreased significantly following excessive scanning of the same region of the sample surface. For the flake shown in Figure 2.7, the height above the Si/SiO_2 substrate was initially measured as ~8 Å. However, after 20 sets of measurements (i.e., scans) on the

same flake, the height was measured as ∼5 Å, as seen in Figure 4.3. The decrease in the height of the single-layer graphene flake above the substrate is due to the fact that the trapped pockets of air/moisture (discussed in Section 2.5) are being pushed away from under the graphene flake by the AFM probe during repeated scanning.

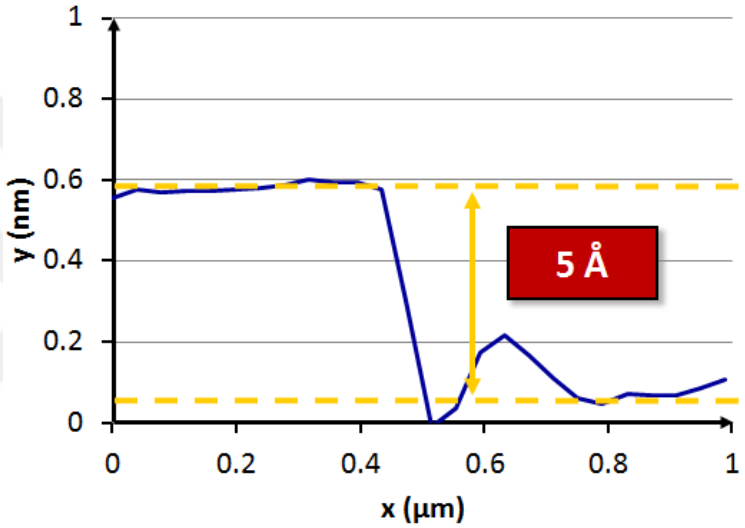

Figure 4.3: Line profile of the same exact region shown in Figure 2.7 after 20 sets of measurements, showing a decrease in topographical height of the associated graphene flake from ∼8 Å to ∼5 Å

4.2 Effect of Number of Layers

Thickness-dependent measurement of friction on graphene, or in other words, the dependence of friction on the number of graphene layers, has been a well-investigated topic in nanotribology research over the last few years [25, 26, 28, 53, 54]. In particular, in certain studies performed on mechanically-exfoliated graphene, it has been shown that friction force values decrease with increasing number of graphene layers, ultimately reaching friction forces measured on bulk graphite which has been found to exhibit considerably less friction than single-layer graphene [26, 54, 55]. The increased friction encountered on graphene

samples with smaller number of layers has been remarkably explained by a phenomenon called "puckering" [26]. The phenomenon of puckering can be visualized as follows: when dragging a finger over a bedsheet, the sheet tends to *aggregate* in front of the finger forming a *bump* or in other words, a *pucker*. This scenario may be thought of analogously to the sharp AFM probe scanning in contact mode over a sheet of graphene. Due to the fact that single-layer graphene does not adhere well to the SiO_2 substrate, it tends to move out of plane in the vertical z-direction when scanned by the AFM probe. This causes an aggregation of graphene (a *pucker*) around the probe apex that is being moved/dragged around when the probe scans the surface, causing additional friction (see Figure 4.4 for an illustration) [26, 52, 56]. For 2-layer graphene this effect is observed less, due to the fact that the stiffness of graphene in the vertical z-direction increases with increasing number of layers, and therefore it becomes harder to make the graphene pucker. Thus, decreasing friction is observed with increasing number of graphene layers, due to increased stiffness and reduced puckering [26]. Additionally, it has been shown that friction on 3 and 4 layers of graphene is almost identical, showing convergence toward bulk graphite behavior [54], as detailed in Figure 4.5 for reference.

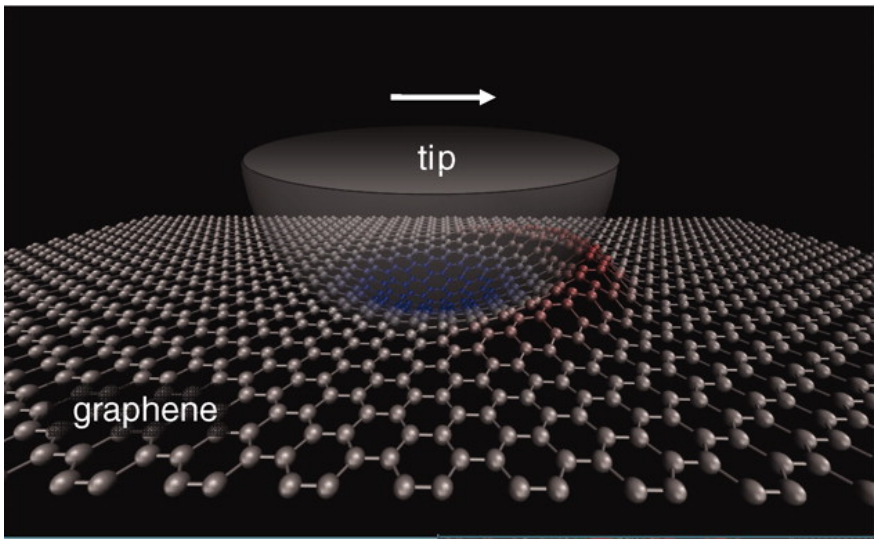

Figure 4.4: Illustration of *puckering* occurring in front of the AFM tip (probe) scanning a single graphene sheet in contact mode [26].

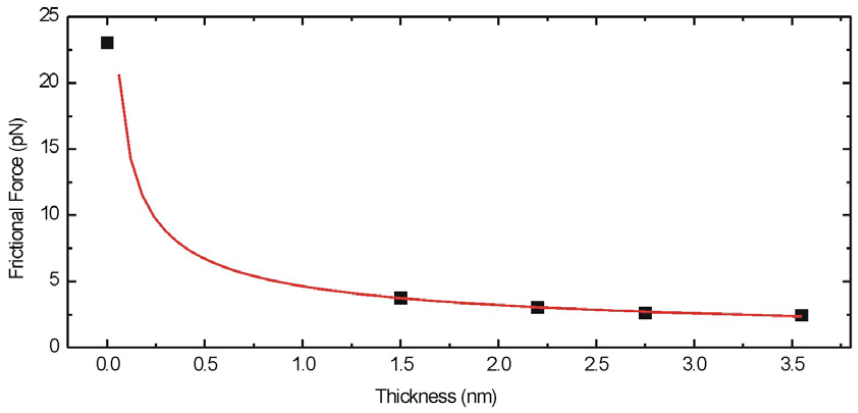

Figure 4.5: Friction force as a function of thickness of graphene/graphite, showing convergence to bulk graphite after thickness values of more than 2-3 layers [54].

At this point, it must be mentioned that the effect of puckering discussed in the previous paragraph in terms of a monotonous decrease in friction with increasing number of graphene layers has been only observed for mechanically-exfoliated graphene samples on Si/SiO_2. On the other hand, measurements performed on graphene grown epitaxially on SiC substrates has shown that 2-layer graphene exhibits lower friction than both single-layer and bulk graphite samples (which was explained by an electron-phonon coupling mechanism) [25, 28]. While a comparison of frictional behavior of graphene samples obtained via different methods is beyond the scope of this thesis, it is hypothesized that the variability in adhesion of graphene to different substrates is responsible for the observed difference in tribological behavior.

In this work, to re-confirm the frictional behavior of mechanically-exfoliated graphene as a function of number of layers as reported in the literature, and form the basis to eventually investigate the possible influence of factors other than puckering on this behavior, AFM-based nanotribology experiments were conducted to quantitatively characterize friction on different graphene samples featuring varying number of layers.

Initially, experimental studies focused on single- and 2-layer graphene flakes as shown in Figure 4.6, due to the fact that they can be easily identified via Raman spectroscopy and can be studied without further structural characterization. As

one can clearly determine from the friction profile shown in Figure 4.5 acquired at an applied load of 0.5 nN, 2-layer graphene indeed exhibits lower friction than single-layer, by about a factor of 2.

For comparison of obtained friction results with multi-layer graphene, flakes which exhibit "stair-like" structures –with 1-2-3-4 layers of graphene present in the same region– were located and structurally identified as explained in Chapter 2. Subsequently, friction measurements as a function of applied load (as explained in the previous section) have been conducted on these samples. In particular, friction force data were obtained and plotted from relatively clean regions (free from contaminants) as marked in Figure 4.7, allowing us to study in detail the trends associated with the effect of number of layers of graphene on its frictional behavior. As one can see from Figure 4.7, the results are in good agreement with the literature, showing decreasing friction (for the same applied load) with increasing number of layers [26, 54]. Finally, it is seen that at higher applied load values the friction force differences on different regions are more pronounced. Therefore, from this point on, when comparing friction, the values obtained at the maximum applied load will be considered.

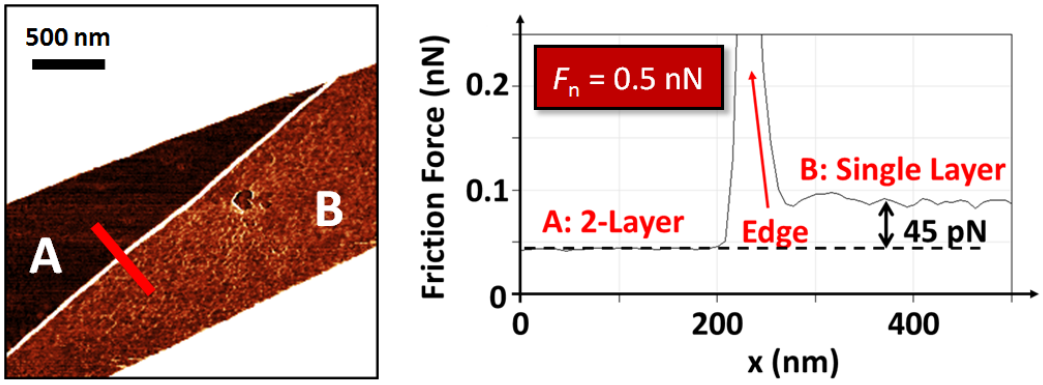

Figure 4.6: Friction force map of a single-/2-layer graphene flake, where the white regions correspond to SiO_2, region A is 2-layer, and region B is single-layer graphene (left). The friction force profile over the red line shows that single-layer graphene exhibits as much as double the friction force on 2-layer graphene (right).

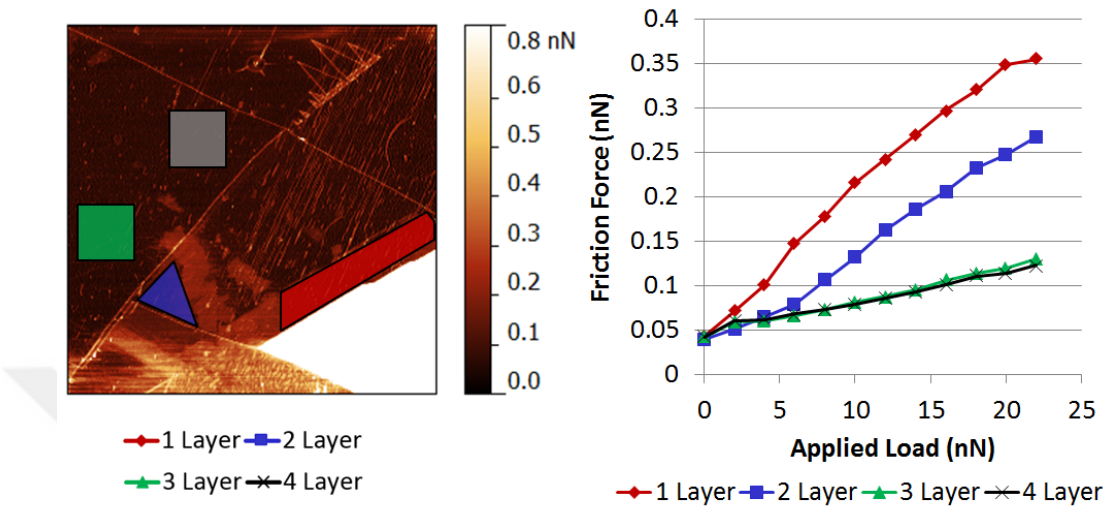

Figure 4.7: Friction force microscopy image of the sample region shown previously in Figure 2.8, where the cleaner regions from which friction data are obtained are highlighted (left). Mean friction force values plotted against applied load and number of layers, as defined by the highlighted regions (right).

4.3 Effect of Tip Radius

At this stage of the experimental work, all results reported in the literature within the context of the nanotribology of mechanically-exfoliated graphene –specifically, the effect of applied load and number of layers on friction– have been successfully reproduced, and quantitatively evaluated. On the other hand, a major experimental parameter, namely the contact area as dictated by the radius of the AFM probe tip, has not been investigated yet in the literature. In fact, interface size is an important design parameter for sliding components featured in micro-/nano-electromechanical devices since adhesive and frictional forces are dependent on surface area and can be dominant factors on such small scales. If graphene is to be used as a solid lubricant in such systems, it is very important that experimentalists determine how its frictional behavior changes as a function of interface size.

Motivated by the discussion above, the dependence of friction forces measured on single- and multi-layer graphene samples on AFM probe tip radius were studied in this thesis. In particular, using the methods described in Chapter 3, AFM

probe tips were modified in size and re-calibrated accordingly. After every increase in the size of the tip radius, the same experiments described in Section 4.2 were repeated on multi-layer flakes, to add the influence of tip radius to the parameter space via which friction is investigated.

Figure 4.8 shows the results of experiments aimed at evaluating friction as a function of applied load, number of graphene layers and now, tip radius. It is seen from the figure that when the tip radius R is doubled (from 40 nm to 80 nm), a significant change in the layer dependence of friction occurs: **(i)** The ratio of friction forces (measured at the maximum applied load of 16 nN) associated with 1-layer and 2-layer graphene regions significantly increases, and remarkably, **(ii)** friction values associated with 2-layer graphene now converge to those of 3- and 4-layer graphene (and thus, to bulk graphite). It must be noted for Figure 4.8 that friction force signal values recorded by the AFM instrument in units of V are reported rather than absolute friction forces in nN. The arguments regarding friction ratios and layer-dependent frictional behavior are, nevertheless, not affected by this particular fact.

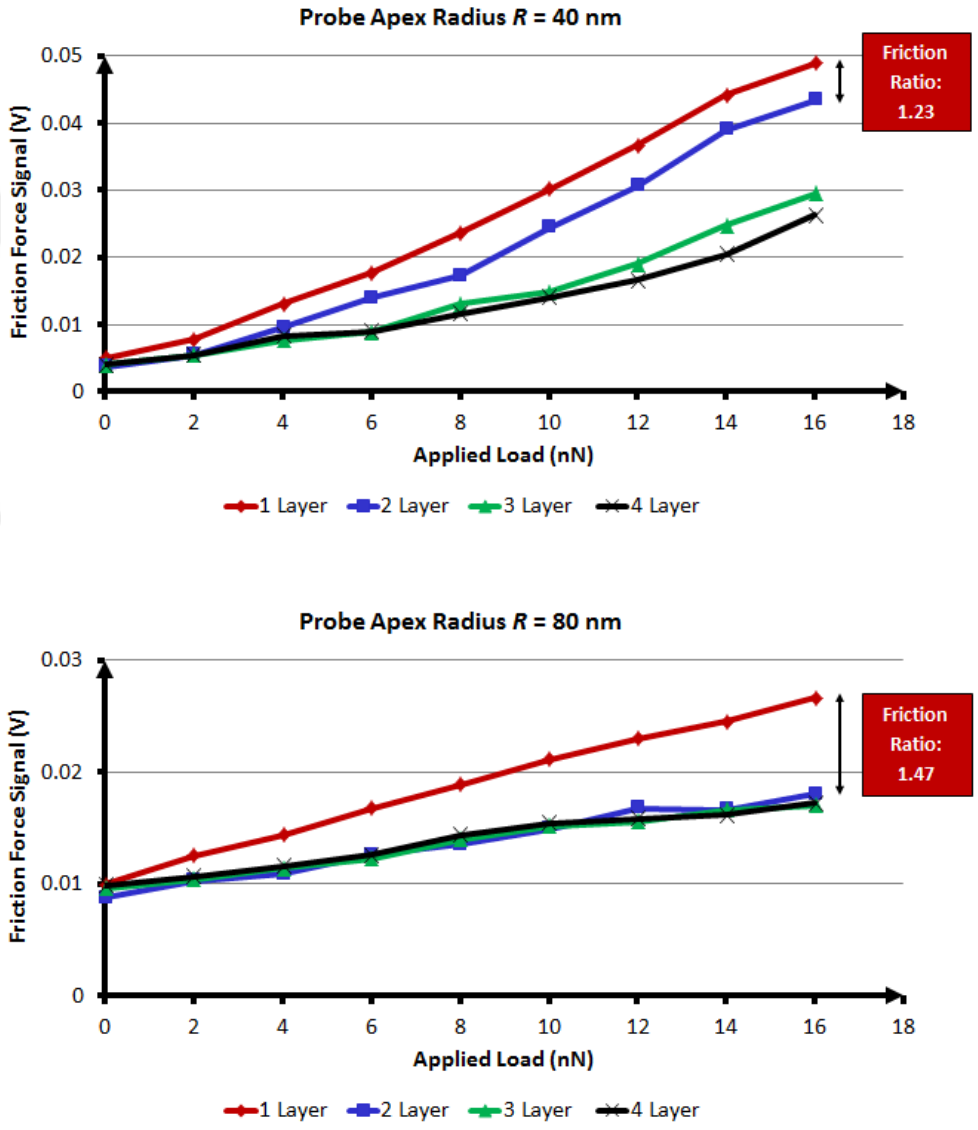

Figure 4.8: Friction force signal plotted against applied load and number of layers, measured with a gold coated tip of 40 nm radius (top), and 80 nm radius (bottom).

The results reported in Figure 4.8 may be interpreted within the framework of the puckering argument discussed in detail in the literature. Specifically, Figure 4.8 points to a drastically decreased effect of puckering starting from two layers of graphene at increasing contact areas (i.e., interface sizes). This finding may be preliminarily and qualitatively understood when one considers that an increase in contact area (tip radius) at the same applied load leads to a smaller pressure on graphene, resulting in a smaller degree of out-of-plane deformation in the z-direction and therefore, less puckering. A more involved quantitative evaluation of this aspect is the subject of future work.

Interestingly, during tip-radius-dependent friction experiments, it has been found that an *increase* in tip radius leads, unexpectedly, to a *decrease* in absolute friction values (in addition to an increase in the 1-to-2-layer friction ratio). Specifically, Figure 4.9 shows friction force values acquired at an applied load of 16 nN on 1-, 2-, 3-layer graphene samples with AFM probes featuring tip radii of 40, 60, and 80 nm. The overall decrease in friction with increasing tip size is clearly observable. To demonstrate that these experimental findings are consistent and reproducible, Fig. 4.10 shows two more sets of measurements, acquired with different AFM probes. Again, the 1-to-2-layer friction ratio is the smallest for the smallest tips and there is an overall (although in one instance, not monotonous) decrease in friction.

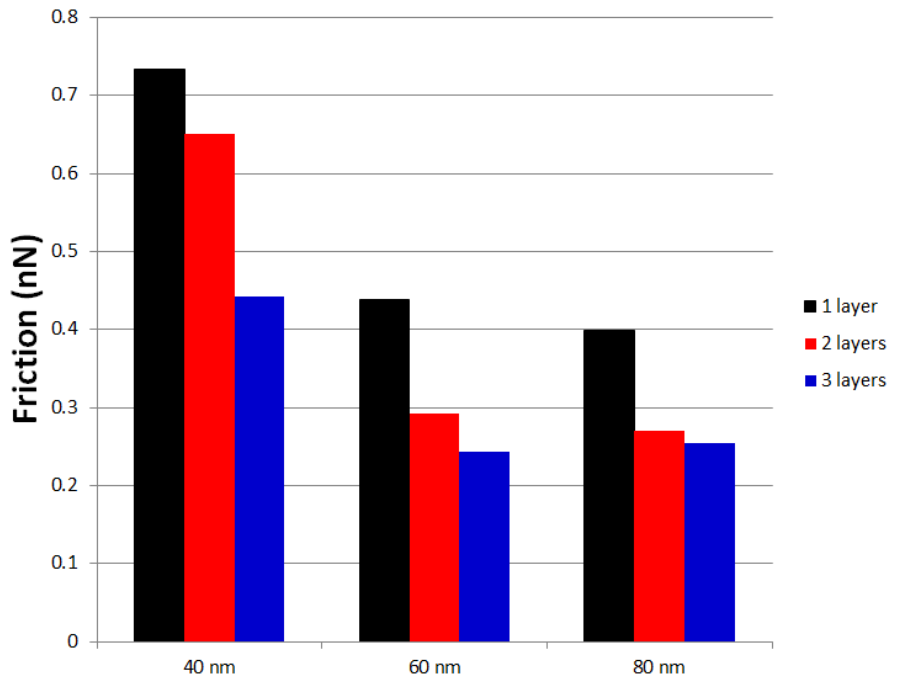

Figure 4.9: Friction force values measured on 1-2-3 layers of graphene with tip radii of 40, 60 and 80 nm. The applied load for these measurements is 16 nN.

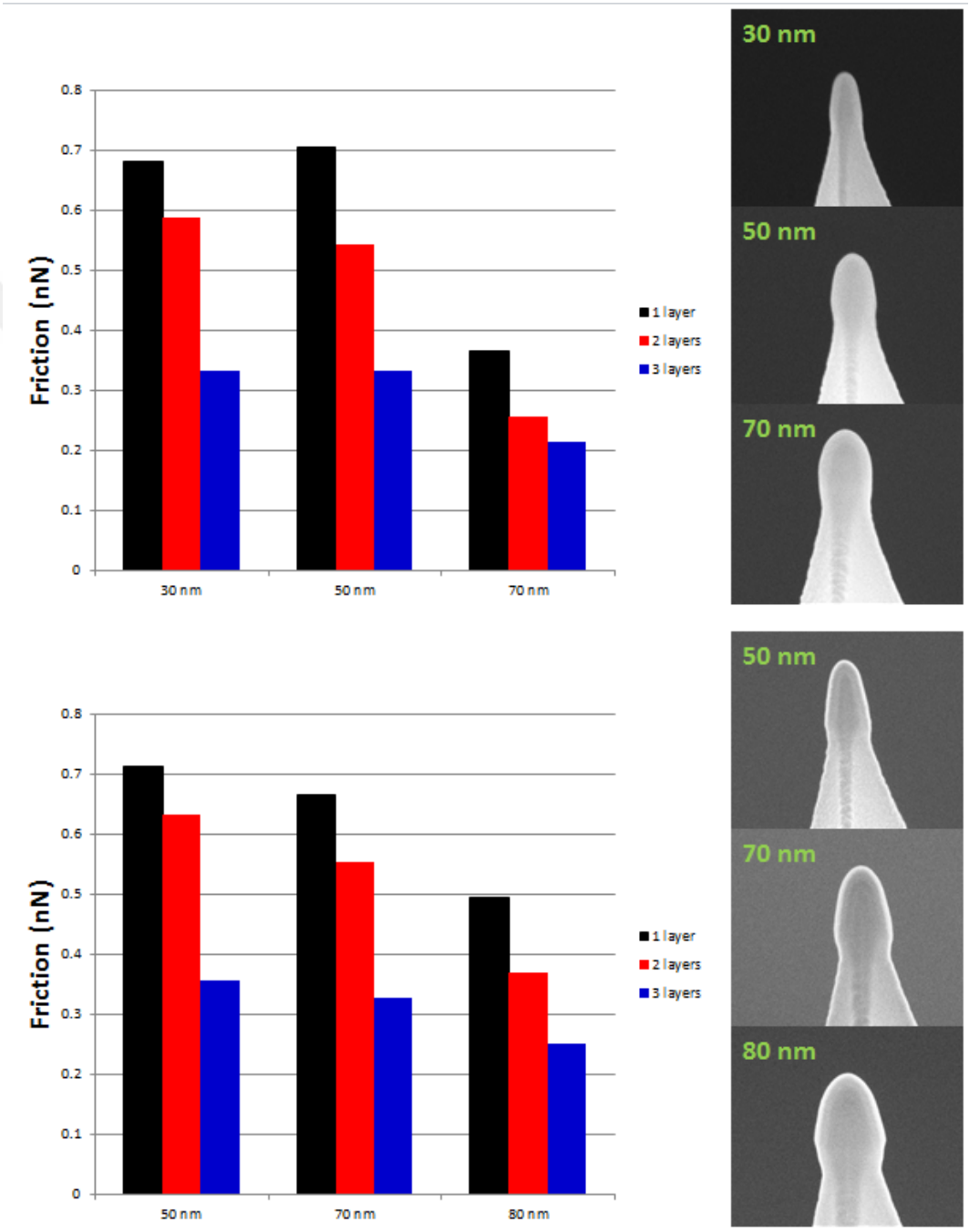

Figure 4.10: Friction force values measured on 1-2-3 layers of graphene with two individual AFM probes featuring tip radii of 30-50-70 nm and 50-70-80 nm, respectively. SEM images of the probe apexes are also provided for reference. The applied load for these measurements is 22 nN.

The overall decrease in friction with increasing tip radius is an unexpected result, since on the nanoscale and on relatively smooth surfaces such as graphene, adhesion is typically thought to be the dominant underlying factor leading to friction [1]. As adhesion increases with increasing contact area, friction is also expected to increase. To experimentally confirm that adhesion on graphene increases with increasing tip radius, *pull-off forces* (corresponding in magnitude to the adhesion between tip and sample) were measured via force spectroscopy on 1-, 2-, and 3-layer graphene regions with two tips of different size and the results are tabulated in Table 4.1.

Table 4.1: Pull-off force values measured on 1-, 2-, 3-layer graphene samples using a 30 nm radius and an 80 nm radius tip.

Layers of Graphene	Pull-off Force (nN)	
	R = 30 nm	R = 80 nm
1	5.3	11.3
2	7.2	11.2
3	6.5	12.1

As seen in Table 4.1, although there is not a significant relation between number of layers and pull-off forces, it is shown that with increasing tip size (contact area), the pull-off force and thus, adhesion indeed increases. This fact points out that there must be another (so far unconsidered) factor that causes the overall decrease in friction with increasing tip size.

4.4 Effect of Interface Roughness

Interface roughness (arising due to the individual roughness of the surfaces forming the interface) is a major factor affecting friction on macro, micro, and nano scales [1]. As already discussed in Chapter 1, all surfaces (even those that appear smooth to the naked eye) are rough on small length scales due to their

multi-asperity character. To characterize surface topography on multiple length scales, conventional parameters such as RMS roughness and correlation length are typically used [57].

While investigating the nanotribological properties of mechanically-exfoliated graphene as a function of various parameters (applied load, number of layers, tip radius) in the previous sections, the observed trends were mostly explained by arguments involving the puckering phenomenon. On the other hand, the influence of interface roughness (caused by both the roughness of the Si/SiO_2 substrate under graphene, as well as the roughness of the AFM probe tip) on frictional behavior has not been investigated.

In this section, we report on our findings involving the effect of interface roughness on the nanotribological properties of graphene. Experimental results are corroborated by MD simulations performed in collaboration with the group of Prof. Ashlie Martini at UC Merced. Specifically, we are able to develop a new point of view with respect to the layer-dependence of friction on graphene that does not involve the puckering effect, and also address the previously-discussed issue of decreasing friction values with larger tips.

4.4.1 Substrate Roughness

In this work, and most other studies of graphene nanotribology reported in the literature, graphene samples are either located on substrates such as Si/SiO_2 and mica, or suspended over micron-sized holes to eliminate substrate-related effects [26, 27, 29, 31, 53]. Since friction at all length scales is expected to be affected by the roughness of the sliding surfaces in contact [1], substrate roughness is naturally expected to play a role in the frictional behavior of graphene, as well. It should be mentioned at this point that graphene layers by themselves are atomically flat, but develop finite corrugations when coated over relatively rough substrates such as Si/SiO_2 due to structural conformation.

To complement our experimental work, we have collaborated with Prof. Ashlie Martini and recent doctoral graduate Zhijiang Ye from UC Merced, who supported our studies with the MD simulations presented in this section, in particular to investigate the effect of substrate roughness on graphene nanotribology. The simulations were performed using the model tip-sample system shown in Figure 4.11, whereby hemispherical tips of different radii consisting of carbon atoms in diamond configuration were slid laterally on 1-, 2- , 3-layer graphene sheets situated on atomically-flat or rough substrates. The inter-atomic interactions within the tip and substrate were described by the popular AIREBO (adaptive intermolecular reactive empirical bond order) potential and the tip-sample interactions were approximated using the Lennard-Jones potential (with an energy minimum of 0.016 eV and zero-crossing distance of 2.8 Å). All simulations were performed at fixed applied loads and scanning speeds of 4 m/s at a temperature of 10 K.

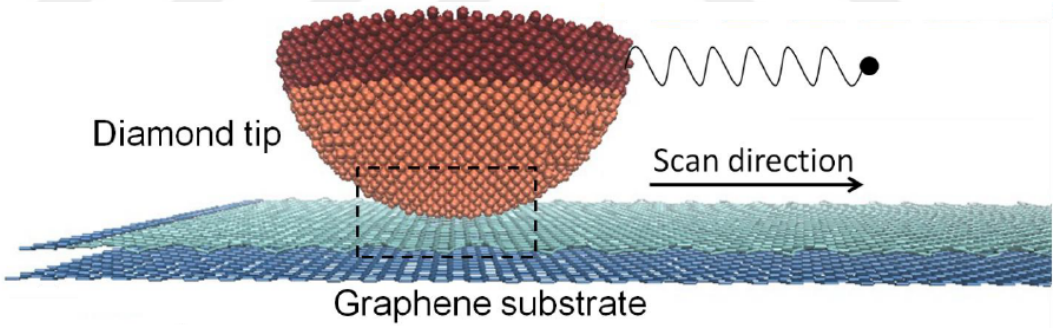

Figure 4.11: Schematic setup for MD simulations whereby a model, hemispherical diamond tip is scanned over a graphene sample to calculate friction forces. While this particular setup visualizes an atomically-flat graphene substrate, simulations may also be performed with substrates featuring realistic roughness values similar to SiO_2.

Results of MD simulations performed in the fashion described above have shown that with a perfectly smooth (i.e., atomically-flat) substrate, the relation between friction and number of layers of graphene is the opposite of what is experimentally observed (see Figure 4.12): Without the presence of substrate roughness, single-layer graphene is expected to demonstrate the lowest friction values, with increasing friction for 2- and 3-layer graphene samples. On the other hand, simulations performed on realistically rough substrates (corresponding to

experimentally measured roughness characteristics of SiO_2: RMS roughness of 3 Å and correlation length of 5 Å) demonstrate the experimentally-observed layer-dependence, whereby friction monotonically decreases with increasing number of layers. These results clearly indicate that substrate roughness plays an important role in the experimentally measured layer-dependence of friction on graphene.

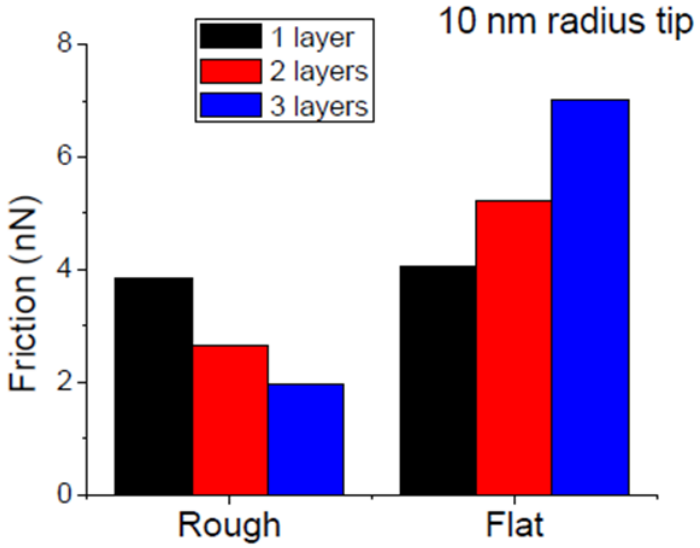

Figure 4.12: Friction trends of graphene with 1, 2, 3 layers on rough and perfectly flat substrates, simulated for a 10-nm radius tip.

The physical interpretation of the simulation results are as follows: On the flat substrate, the dominating effect dictating friction is expected to be graphene deformation (i.e., puckering): With a perfectly flat substrate the separation between graphene layers are minimized (meaning that each layer can perfectly conform to the one below); therefore when pushed towards the graphene surface, not only the top layer of graphene, but also the layer below can adhere reasonably well to the probe tip. Consequently, when more layers of graphene are present, more material is moved around by the scanning probe tip via puckering, and a higher friction value is calculated. However on a rough (i.e., not atomically-flat and therefore, realistic) substrate, graphene cannot fully conform to the underlying topography [58]. Additionally, while the first graphene layer demonstrates the highest roughness, the conformity to substrate roughness decreases with increasing number of layers, leading to a reduction in topographical surface corrugation (Figure 4.13) and thus, resulting in lower friction. This result puts forth the idea

that experimentally observed high friction of single-layer graphene is not caused by puckering alone, but also the high surface roughness when compared with graphene featuring two layers or more.

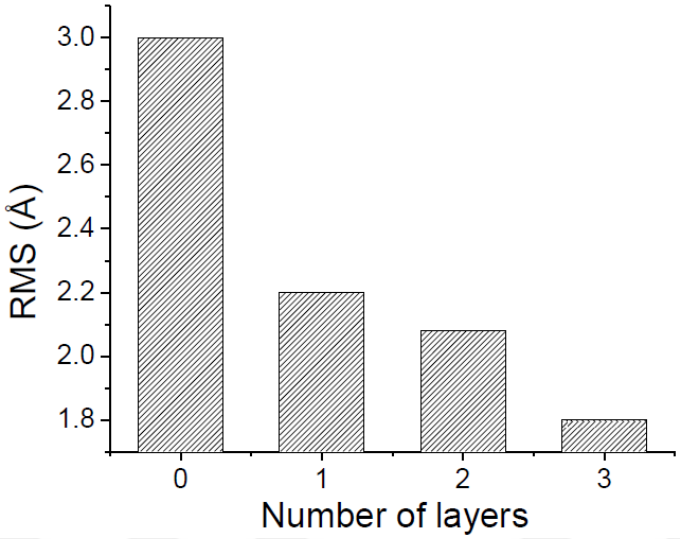

Figure 4.13: Numerically-calculated values of the RMS roughness of the top layer of graphene for 1-, 2-, and 3-layer samples. "0" designates the SiO_2 substrate.

To study the cross-over from deformation-dominated to roughness-dominated frictional behavior of graphene in more detail, MD simulations have been performed that show the effect of changing substrate topography (in terms of changing correlation length at a fixed RMS roughness of 3 Å) on the frictional behavior of graphene (Figure 4.14). It should be noted here that higher correlation length values mean that the substrate is more "flat", taking into account the ratio between the probe tip size and the lateral separation of asperities on the substrate (as determined by the correlation length). The red-shaded region in Figure 4.14 thus corresponds to the roughness-dominated regime where the correlation length of the substrate is small, and the layer-dependence trend is in agreement with all experimental results in the literature (including ours). The blue-shaded region is the deformation-dominated region where the substrate is closer to an ideally (i.e., atomically) flat surface and the layer trend is reversed, as discussed earlier. Finally the yellow-shaded region corresponds to the cross-over regime where no consistent trend in terms of layer dependence of friction is observed.

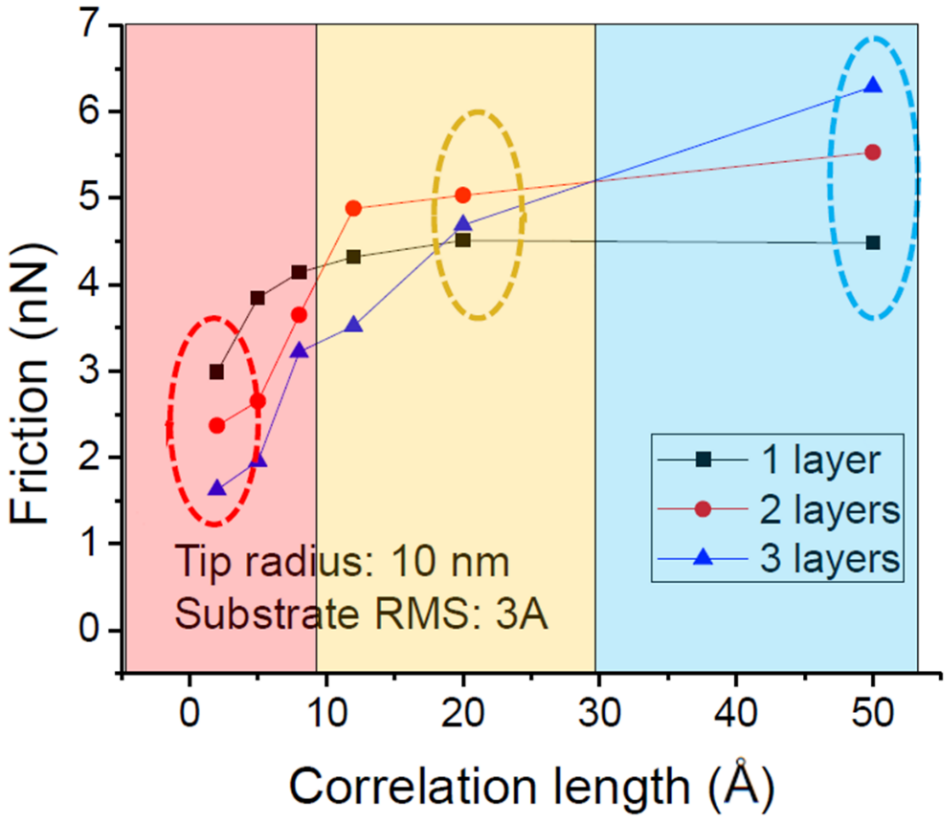

Figure 4.14: Results of MD simulations that illustrate the cross-over from roughness-dominated to deformation-dominated layer-dependent frictional behavior of graphene.

To experimentally confirm the changes in substrate roughness with changing number of graphene layers as predicted by MD simulations, RMS roughness values were measured on 1-, 2-, 3-, and 4-layer graphene samples via 100 different topographical AFM scans. The related results are presented in Figure 4.15. As it can be seen clearly from the figure, AFM experiments demonstrate that RMS roughness values associated with graphene indeed decrease with increasing number of layers, in accordance with the simulations. One notable exception is the increase in RMS roughness recorded for single-layer graphene when it is coated on SiO_2. The physical reason for this observation is the existence of pockets of trapped air/moisture between SiO_2 and the first graphene layer, which do not exist in the simulations.

In order to experimentally observe the reversed layer-dependence of friction

predicted for graphene samples situated on flat substrates, we have conducted experiments on graphene exfoliated onto mica (which is expected to be flatter than SiO_2). While experiments confirmed that RMS roughness values for mica substrates are indeed lower than those for SiO_2, the difference was dictated only by a factor of 2 and as such, no significant deviation in frictional behavior was observed for these samples when compared to those on SiO_2.

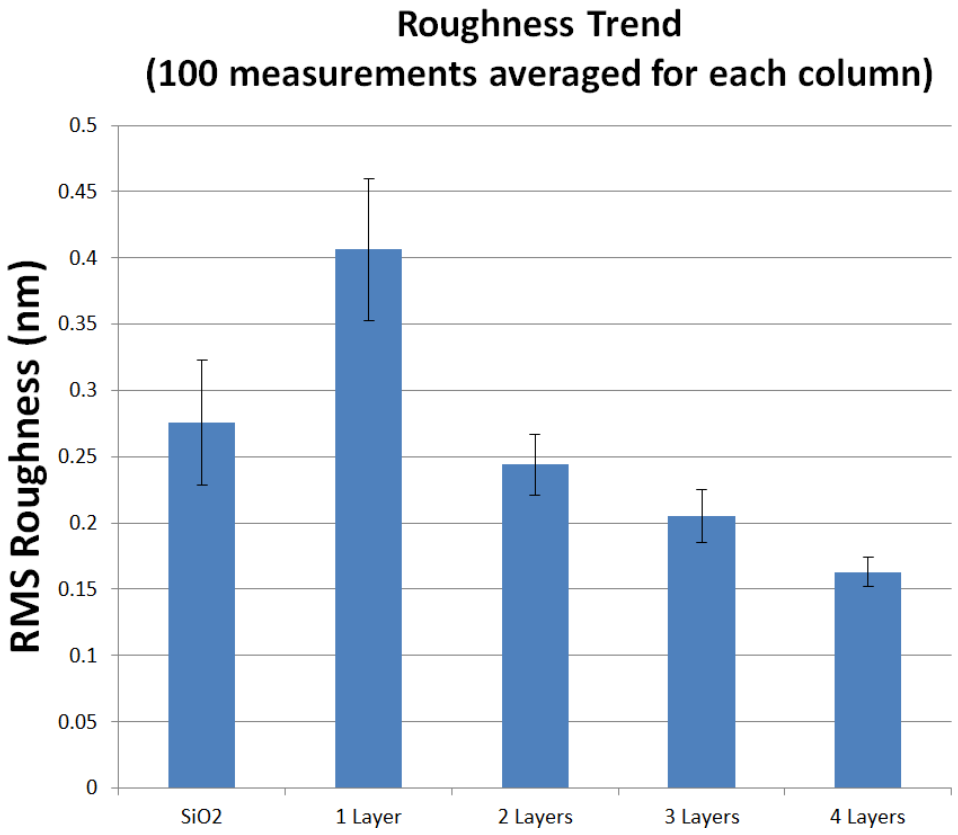

Figure 4.15: Experimentally measured RMS roughness values for the SiO_2 substrate as well as graphene samples of varying number of layers.

4.4.2 Tip Roughess

An important observation that was reported in Section 4.3 was that the overall friction values kept decreasing with increasing tip sizes. As already discussed, this is unexpected, as larger contact areas typically lead to more friction in conjunction with increased adhesion. In order to shed light on this issue, MD simulations

aimed at determining layer-dependent friction values on graphene as a function of tip size have been performed (Figure 4.16). While the results confirm the experimentally observed trend that the 1-to-2-layer friction ratio increases with tip size (see dashed arrows), no decreasing trend in friction with increasing tip size is observed.

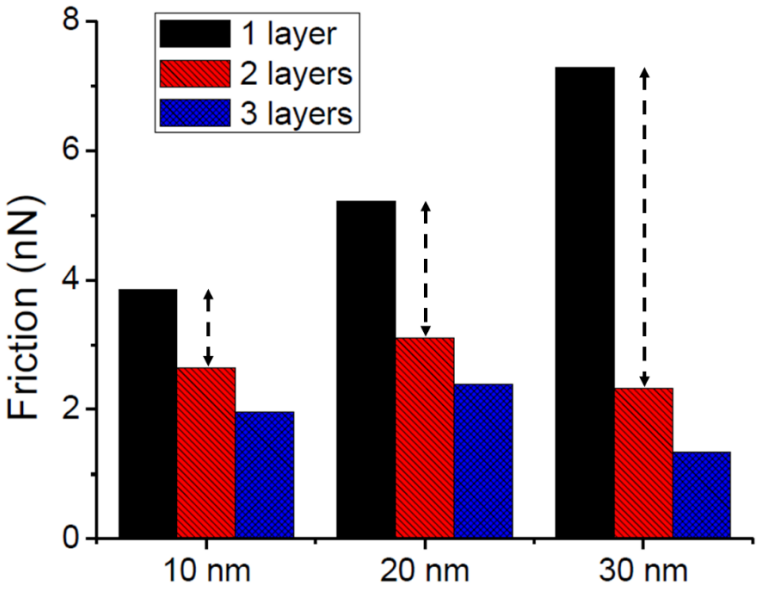

Figure 4.16: Friction forces calculated via MD simulations performed on 1-, 2-, 3-layer graphene samples with tips having radii of 10, 20, and 30 nm. Dashed arrows designate the 1-to-2-layer friction ratio that increases with tip size, confirming experimental observations. On the other hand, contrary to experiments, friction forces show an overall increase with increasing tip size.

At this point, all parameters employed in the experiments and simulations (tip size, applied load, number of layers, substrate roughness, etc.) did match except one that we cannot measure experimentally: The *roughness of the tip.* While the simulations involve a perfectly (i.e., atomically) smooth, hemi-spherical tip geometry, AFM probes used in the experiments are always coated with gold, which could presumably alter roughness on the nanometer scale and below.

Since SEM imaging of AFM probes does not yield high-enough resolution with which probe roughness may be quantified, we have turned our attention to published studies in the literature regarding the relationship between thermal

evaporation of gold and resulting topography. In particular, an AFM-based experimental study shows that when gold coating is performed at low thickness values (<20 nm) the surface is not uniformly coated and rather globular structures of gold are formed on the surface, which exhibit high roughness values when compared with thicker coatings (>30 nm) which have more uniform and smoother distribution of gold over the surface (Figure 4.17) [59].

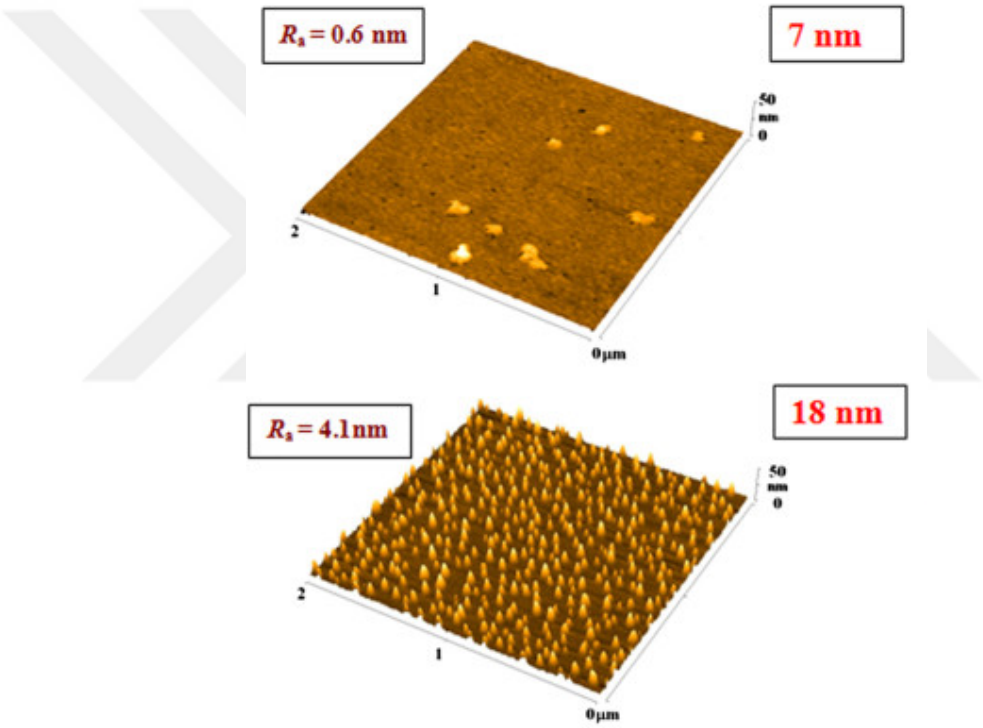

Figure 4.17: Topographical AFM scan of a SiO_2 surface coated with 18 nm of gold, showing separated globular structures causing a high surface roughness (R_a) (top). Topographical AFM scan of a SiO_2 surface coated with 35 nm of gold, showing a more uniform and smoother surface topography [59].

In our experiments, the initial coating of gold performed on AFM probes is ∼15 nm thick and therefore is expected to be rough. As more gold is coated onto a particular tip to increase its radius, the surface of the tip becomes more uniformly coated and therefore, smoother. Thus, the initially-high roughness of the gold-coated tip surface may explain why smaller tips consistently exhibit higher overall friction when compared with larger tips, as shown in Section 4.3.

Chapter 5

Summary and Outlook

The work presented in this M.S. thesis first covers the fabrication and identification of mechanically-exfoliated graphene, as well as the calibration and modification of contact-mode atomic force microscopy probes. Subsequently, a comprehensive investigation of the nanotribological properties of mechanically-exfoliated graphene via atomic force microscopy (AFM) is presented, whereby special emphasis is placed on the effect of interface structure. Remarkably, presented experimental results provide a new perspective towards the layer-dependent frictional behavior of graphene, underlining the influence of substrate roughness in addition to the phenomenon of *puckering* that is well-studied in the literature.

Graphene samples ranging from single- to few-layers have been obtained using the mechanical exfoliation method and transferred onto Si/SiO_2 substrates. By utilizing optical microscopy and Raman spectroscopy, graphene flakes exhibiting single- and bi-layer regions were located and identified. Furthermore, using topographical maps and associated profiles obtained via AFM, 3-, 4-layer and bulk graphite regions were found. Moreover, AFM probes were calibrated both for accurate normal force readings, and for obtaining quantitative friction force data from lateral force measurements conducted via contact-mode AFM under ambient conditions.

After sample preparation, identification and probe calibration, experiments aimed at measuring the effect of applied load on friction of single-layer graphene were conducted, which reproduced the results in literature. Subsequently, measurements were performed on 2-, 3-, 4-layers graphene for quantitative comparison in terms of frictional behavior, again confirming previous results reported in the literature showing increased friction on fewer layers of graphene an observation which is commonly explained by the puckering phenomenon. The third parameter that was investigated in this work in terms of its effect on graphene's frictional behavior was the tip radius. In particular, thermal evaporation- and PECS-based coating of gold onto AFM probes were utilized to modify tip radii. Decreasing trends in overall friction were observed with increasing tip size, which led to the determination of a new parameter affecting friction on graphene: interface roughness. In collaboration with scientists from UC Merced, who performed molecular dynamics (MD) simulations complementing the experiments presented here, it was determined that increased friction on fewer layers of graphene is caused by the roughness of the substrate leading to the first graphene layer to feature a certain topographical corrugation, as well. Structural conformity to the substrate (and consequently, topographical corrugation) decreases with each subsequent graphene layer, resulting in reduced friction with increasing number of layers. This effect may be in addition to, or dominant over, the puckering phenomenon that has been studied in detail in the literature.

Even though the experimental results presented in this work comprehensively cover major influences of interface structure on the frictional behavior of graphene, further experiments have to be conducted to fully evaluate graphene's suitability for use as a solid lubricant in micro-/nano-electromechanical devices. Specifically, experiments following up on the effects of **(i)** using different types of materials for coating probe tips (e.g., platinum) and **(ii)** using different substrates with smoother topographies (such as individual, detached graphene flakes on bulk graphite [60]) would provide crucial information. Within this context, we are of the opinion that this thesis will provide a major step forward in characterizing the frictional behavior of mechanically-exfoliated graphene and accelerate its practical application as a solid lubricant in micro- and nano-scale systems.

Bibliography

[1] B. Bhushan, "Introduction to Tribology," *Wiley*, New York, 2013.

[2] B. Bhushan, "Principles and applications of tribology," *Wiley*, New York, 1999.

[3] P. J. Blau, "Friction science and technology: from concepts to applications," *CRC Press*, Boca Raton, 2009.

[4] T. Mang, K. Bobzin and T. Bartels, "Industrial tribology: tribosystems, friction, wear and surface engineering, lubrication," *Wiley-VCH*, Weinheim, 2011.

[5] D. Dowson, "History of Tribology," *Professional Engineering Publishing*, London, 1998

[6] G. Amontons, "De la resistance cause e dans les machines," *Mémoires de l'Académie Royale A*, pp. 275282, 1699.

[7] J. Krim, "Surface science and the atomic-scale origins of friction: what once was old is new again," *Surface Science*, vol. 500, no.1-3, pp. 741-758, 2002.

[8] J.A. Greenwood and J. B. P. Williamson, "Contact of Nominally Flat Surfaces," *Proceedings of the Royal Society of London A*, vol. 295, pp. 300-319, 1966.

[9] G. Binnig, C. F. Quate and C. Gerber, "Atomic force microscope," *Physical Review Letters*, vol. 56, no. 9, pp. 930-933, 1986.

[10] C. M. Mate, G. M. Mcclelland, R. Erlandsson and S. Chiang, "Atomic-scale friction of a tungsten tip on a graphite surface," *Physical Review Letters*, vol. 59, no. 17, pp. 1942-1945, 1987.

[11] Szlufarska, M. Chandross and R. W. Carpick, "Recent advances in single-asperity nanotribology," *Journal of Physics D: Applied Physics*, vol. 41, pp.123001, 2008.

[12] G. Binnig, H. Rohrer, C. Gerber and E. Weibel, "Surface studies by scanning tunneling microscopy," *Physical Review Letters*, vol. 49, no. 1, pp. 57-61, 1982.

[13] P. Eaton and P. West, "Atomic Force Microscopy," *Oxford University Press*, New York, 2010.

[14] PSIA Corp., "XE-100 Users Manual," 2002.

[15] U. D. Schwarz, P. Koster and R. Wiesendanger, "Quantitative analysis of lateral force microscopy experiments," *Review of Scientific Instruments*, vol. 67, no. 7, pp. 2560-2567, 1996.

[16] K. S. Novoselov, A. K. Geim, S. V. Morozov, D. Jiang, Y. Zhang, S. V. Dubonos, I. V. Grigorieva and A. A. Firsov "Electric field effect in atomically thin carbon films," *Science*, vol. 306, no. 5696, pp. 666-669, 2004.

[17] A. K. Geim and K. S. Novoselov, "The rise of graphene," *Nature Materials*, vol. 6, no. 5934, pp. 183-191, 2007.

[18] A. K. Geim, "Graphene: status and prospects," *Science*, vol. 324, no. 5934, pp. 1530-1534, 2009.

[19] A. Kumar and C. Huei, "Synthesis And Biomedical Applications Of Graphene: Present And Future Trends," *Advances in Graphene Science*, doi: 10.5772/55728, 2013.

[20] K. S. Novoselov, D. Jiang, F. Schedin, T. J. Booth, V. V. Khotkevich, S. V. Morozov and A. K. Geim, "Two-dimensional atomic crystals," *Proceedings of the National Academy of Sciences*, vol. 102, no. 30, pp. 10451-10453, 2005.

[21] K. S. Novoselov, A. K. Geim, S. V. Morozov, D. Jiang, M. I. Katsnelson, I. V. Grigorieva, S. V. Dubonos and A. A. Firsov, "Two-dimensional gas of massless Dirac fermions in graphene," *Nature*, vol. 438, no. 7065, pp. 197-200, 2005.

[22] C. Lee, X. Wei, J. W. Kysar and J. Hone, "Measurement of the elastic properties and intrinsic strength of monolayer graphene," *Science*, vol. 321, no. 5887, pp. 385-388, 2008.

[23] D. Berman, A. Erdemir and A. V. Sumant, "Graphene: a new emerging lubricant," *Materials Today*, vol. 17, no. 1, pp. 31-42, 2014.

[24] K. S. Kim, H. Lee, C. Lee, S. Lee, H. Jang, J. Ahn, J. Kim and H.Lee, "Chemical vapor deposition-grown graphene: the thinnest solid lubricant," *ACS Nano*, vol. 5, no. 6, pp. 5107-5114, 2011.

[25] T. Filleter, J. L. Mcchesney, A. Bostwick, E. Rotenberg, K. V. Emtsev, Th. Seyller, K. Horn and R. Bennewitz, "Friction and dissipation in epitaxial graphene films," *Physical Review Letters*, vol. 102, no. 8, pp. 086102, 2009.

[26] C. Lee, Q. Li, W. Kalb, X. Z. Liu, H. Berger, R. W. Carpick and J. Hone, "Frictional characteristics of atomically thin sheets," *Science*, vol. 328, no. 5974, pp. 76-80, 2010.

[27] T. Demirba and M. Z. Baykara, "Nanoscale tribology of graphene grown by chemical vapor deposition and transferred onto silicon oxide substrates," *Journal of Materials Research*, doi: 10.1557/jmr.2016.11, 2016.

[28] T. Filleter and R. Bennewitz, "Structural and frictional properties of graphene films on SiC (0001) studied by atomic force microscopy," *Physical Review B*, vol. 81, no. 15, pp. 155412, 2010.

[29] Y. Peng, Z. Wang and C. Li, "Study of nanotribological properties of multilayer graphene by calibrated atomic force microscopy," *Nanotechnology*, vol. 25, no. 30, pp. 305701, 2014.

[30] P. Egberts, G. H. Han, X. Z. Liu, A. T. C. Johnson and R. W. Carpick, "Frictional behavior of atomically thin sheets: hexagonal-shaped graphene

islands grown on copper by chemical vapor deposition," *ACS Nano*, vol. 8, no. 5, pp. 5010-5021, 2014.

[31] G. Fessler, B. Eren, U. Gysin, T. Glatzel and E. Meyer, "Friction force microscopy studies on SiO2 supported pristine and hydrogenated graphene," *Applied Physics Letters*, vol. 104, no. 4, pp. 041910, 2014.

[32] R. H. Savage, "Graphite lubrication," *Journal of Applied Physics*, vol. 19, no. 1, pp. 1-11, 1948.

[33] F. P. Bowden and J. E. Young, "Friction of diamond, graphite, and carbon and the influence of surface films," *Proceedings of the Royal Society A*, vol. 208, no. 1095, pp. 444-455, 1951.

[34] V. Berry, "Impermeability of graphene and its applications," *Carbon*, vol. 62, pp. 1-10, 2013.

[35] "Piranha Solutions." [Online]. Available: https://ehs.princeton.edu/laboratory-research/chemical-safety/chemical-specific-protocols/piranha-solutions

[36] F. Rozploch, J. Patyk and J. Sankowski, "Graphenes Bonding Forces in Graphite," *Acta Physica Polonica A*, vol. 112, no. 3, pp. 557-562, 2007.

[37] A. R. Rao, V. Hanchanale, P. Javle, O. Karim and H. Motiwala, "Spectroscopic view of life and work of the Nobel laureate sir C.V. Raman," *Journal of Endourology*, vol. 21, no. 1, pp. 8-11, 2007.

[38] C. S. S. R. Kumar, "Raman spectroscopy for nanomaterials characterization," *Springer*, Berlin, 2012.

[39] A. C. Ferrari, J. C. Meyer, V. Scardaci, C. Casiraghi, M. Lazzeri, F. Mauri, S. Piscanec, D. Jiang, K. S. Novoselov, S. Roth and A. K. Geim, "Raman spectrum of graphene and graphene layers," *Physical Review Letters*, vol. 97, no. 18, pp. 187401, 2006.

[40] T. Oznuluer, E. Pince, E. O. Polat, O. Balci, O. Salihoglu and C. Kocabas, "Synthesis of graphene on gold," *Applied Physics Letters*, vol. 98, no. 18, pp. 183101, 2011.

[41] J. E. Sader, I. Larson, P. Mulvaney and L. R. White, "Method for the calibration of atomic force microscope cantilevers," *Review of Scientific Instruments*, vol. 66, no. 7, pp. 3789-3798, 1995.

[42] "AFM Probes, Atomic Force Micrscope tips." [Online]. Available: http://www.nanosensors.com

[43] "AFM probes, AFM tips, AFM cantilevers." [Online]. Available: http://www.budgetsensors.com

[44] D. F. Ogletree, R. W. Carpick and M. Salmeron, "Calibration of frictional forces in atomic force microscopy," *Review of Scientific Instruments*, vol. 67, no. 9, pp. 3298-3306, 1996.

[45] M. Varenberg, I. Etsion and G. Halperin, "An improved wedge calibration method for lateral force in atomic force microscopy," *Review of Scientific Instruments*, vol. 74, no. 7, pp. 3362-3367, 2003.

[46] J. Goldstein, D. E. Newbury, D. C. Joy, C. E. Lyman, P. Echlin, E. Lifshin, L. Sawyer and J. R. Michael, "Scanning electron microscopy and X-ray microanalysis," *Springer*, Berlin, 2003.

[47] U. D. Schwarz, O. Zwrner, P. Kster and R. Wiesendanger, "Preparation of probe tips with well-defined spherical apexes for quantitative scanning force microscopy," *Journal of Vacuum Science & Technology B*, vol. 15, no. 4, pp. 1527-1530, 1997.

[48] B. Hammer and J. K. Nrskov, "Why gold is the noblest of all the metals," *Nature*, vol. 376, pp. 238-240, 1995.

[49] Z. Deng, A. Smolyanitsky, Q. Li, X. Feng and R. J. Cannara, "Adhesion-dependent negative friction coefficient on chemically modified graphite at the nanoscale," *Nature Materials*, vol. 11, pp. 1032-1037, 2012.

[50] H. L. Skriver, and N. M. Rosengaard, "Surface Energy and Work Function of Elemental Metals," *Physical Review B*, vol. 46, pp. 7157-7168, 1992.

[51] J. S. Choi, J. S. Kim, I. S. Byun, D. H. Lee, M. J. Lee, B. H. Park, C. Lee, D. Yoon, H. Cheong, K. H. Lee, Y. W. Son, J. Y. Park, M. Salmeron, "Friction Anisotropy-Driven Domain Imaging on Exfoliated Monolayer Graphene," *Science*, vol. 333, no. 6042, pp. 607-610, 2011.

[52] Z. Ye and A. Martini, "Atomistic Simulation of the Load Dependence of Nanoscale Friction on Suspended and Supported Graphene," *Langmuir*, vol. 30, no. 49, pp. 14707-14711, 2014.

[53] Q. Li, C. Lee, R. W. Carpick and J. Hone, "Substrate effect on thickness dependent friction on graphene," *Physica Status Solidi B*, vol. 247, no. 11-12, pp. 2909-2914, 2010.

[54] H. Lee, N. Lee, Y. Seo, J. Eom and S. Lee, "Comparison of frictional forces on graphene and graphite," *Nanotechnology*, vol. 20, no. 32, pp. 325701, 2009.

[55] M. Dienwiebel, G. S. Verhoeven, N. Pradeep, J. W. M. Frenken, J. A. Heimberg and H. W. Zandbergen, "Superlubricity of graphite," *Physical Review Letters*, vol. 92, no. 12, pp. 126101, 2004.

[56] Z. Ye, C. Tang, Y. Dong and A. Martini, "Role of wrinkle height in friction variation with number of graphene layers," *Journal of Applied Physics*, vol. 112, no. 11, pp. 116102, 2012.

[57] B. Bhushan, J. N. Israelachvili and U. Landman, "Nanotribology: friction, wear and lubrication at the atomic scale," *Nature*, vol. 374, no. 6523, pp. 607-616, 1995.

[58] J. C. Spear, J. P. Custer and J. D. Batteas, "The influence of nanoscale roughness and substrate chemistry on the frictional properties of single and few layer graphene," *Nanoscale*, vol. 7, no. 22, pp. 10021-10029, 2015.

[59] A. Schaub, P. Slepika, I. Kaprkov, P. Malinsk, A. Mackov and V. vork. "Gold Nanolayer and Nanocluster Coatings Induced by Heat Treatment and Evaporation Technique," *Nanoscale Research Letters*, vol. 8, no. 1, pp. 249, 2013.

[60] E. Koren, E. Lrtscher, C. Rawlings, A. W. Knoll and U. Duerig, "Adhesion and friction in mesoscopic graphite contacts," *Science*, vol. 348, no. 6235, pp. 679-683, 2015.